ASSESSING LATERAL TRANSPORT AS A SOURCE OF SCATTER IN THE GLOBAL TEX$_{86}$-SST CALIBRATION: A CASE STUDY FOR THE SOUTH ATLANTIC OCEAN

5/20/2021

MASTER THESIS MARINE SCIENCES
UTRECHT UNIVERSITY

STUDENTS : **MOHAMMAD RIZKY NANDA HADJU**
NUMBER : **6307515**
ECTS : **45**
CORRECTORS : **Dr. Ir. FRANCIEN PETERSE**
Dr. PETER BIJL
ADDISON RICE, M.Sc
PETER NOOTEBOOM, M.Sc
Dr. ERIK VAN SEBILLE

MSc Research (GEO4-1521)

Assessing Lateral Transport as a Source of Scatter in the Global TEX_{86}-SST Calibration: a Case Study for the South Atlantic Ocean

Abstract

TEX_{86} (Tetraether index of tetraethers, which contains 86 carbon atoms) is a valuable proxy for absolute Sea Surface Temperature (SST) reconstructions. However, scatter in the relationship between sedimentary TEX86 ratios and the SST of the overlying water cause large calibration error bars in reconstructions. Hence, understanding the exact relationship between SST and sedimentary TEX_{86} index values might help reduce such calibration error bars. One of the questions is to what extent ocean currents laterally displace descending GDGTs-bearing particles through the water column. The GDGTs transport during sinking was simulated in a high-resolution model of the Subtropical South Atlantic of the modern ocean. The simulations allowed quantification of an offset between the region of origin of these particles and the directly overlying water. At several sinking speeds, the particles were tracked back from the position of the surface sediment sample to a water depth of 30 meter. Crucially, this has been concluded that water depth and the ratio between GDGTs bearing two vs. three cyclopentyl moieties ([2]/[3] ratio) reflecting a contribution from Archaea living in deeper waters are better discriminators of ΔSST bias values (an offset between the TEX_{86}-derived SST and modeled average SST of transported particles) than lateral transport itself in the South Atlantic Ocean sub-dataset. Since lateral transport-related SST changes with water depth, it is no longer representative of directly overlying SST; the deeper the site, the larger ΔSST bias with the signal of the directly overlying water. It was also found that the shallow sites (<1000 m) have been consistent cold offset while the deeper sites (>1000 m) consistently have a warmer bias with a high [2]/[3] ratio. However, the lateral transport effect can be best seen if looked at a specific region, as ΔSST (the TEX_{86}-derived SST (SST_{TEX86}) – modeled-overlying SST) is also a function of travel distance of particles, influencing the signal. The prevailing ocean current in the Southeast Atlantic is Agulhas Current while the Southwest Atlantic is induced by two currents coming from the Southern Ocean and dominantly from Brazilian Current (from the Equatorial Current), causing a cold ΔSST bias. This is a surprising observation due to the transport effect, yielding markedly elevated temperatures difference in some sites, ultimately affecting the calibration. A few aspects such as possible local events in the ocean which might cause an anomaly, the depth productivity, sub-sea surface temperature, the horizontal travel distance bias of the particles before sinking, and a global scale simulation need to be taken into account for future efforts.

1. INTRODUCTION

Isoprenoid glycerol dibiphytanyl glycerol tetraethers (isoGDGTs) are membrane lipids of archaea, characterized by monolayers of isoprenoid chains ether-bound to glycerol backbones (Schouten et al., 2013 for a review). The isoGDGTs with up to 8 cyclopentane moieties have been found in a variety of ancient and modern sediments (Fig. 1). An isoGDGT with four cyclopentane moieties and one cyclohexane moiety is named crenarchaeol and seems to be exclusively produced by ammonia oxidizing Thaumarchaeota (DeLong et al., 1998; de la Torre et al., 2008; Pitcher et al., 2010). The degree of cyclisation of isoGDGTs is related to temperature. Culture studies with thermophilic archaea showed that the number of cyclopentane moieties increases with rising temperature (DeRosa et al., 1980; Uda et al., 2001, 2004). The same observation was made in the marine environment, where GDGTs in marine surface sediments at higher latitudes, and thus lower SST, contain fewer cyclopentane moieties than those at lower latitudes, and thus higher SST (Schouten et al., 2002). Based on this observation, the TEX_{86} (Tetraether index of tetraethers, which contains 86 carbon atoms) (*see equation (1)*) was introduced to quantify the relation between temperature (SST) and isoGDGT distributions (Schouten et al., 2002). The different GDGT membrane lipids preserved in sediment show a historical pattern of their abundance. Since these cyclopentane rings are able to enhance the integrity structurally and the resistance of the ether-bound monolayer towards heat stress (Wucher et

al., 2004), the TEX_{86} proxy, based on the relative abundance of cyclopentane moieties in GDGTs of Crenarchaeotal membrane lipids, has been a focus for scientists as a reliable paleothermometer.

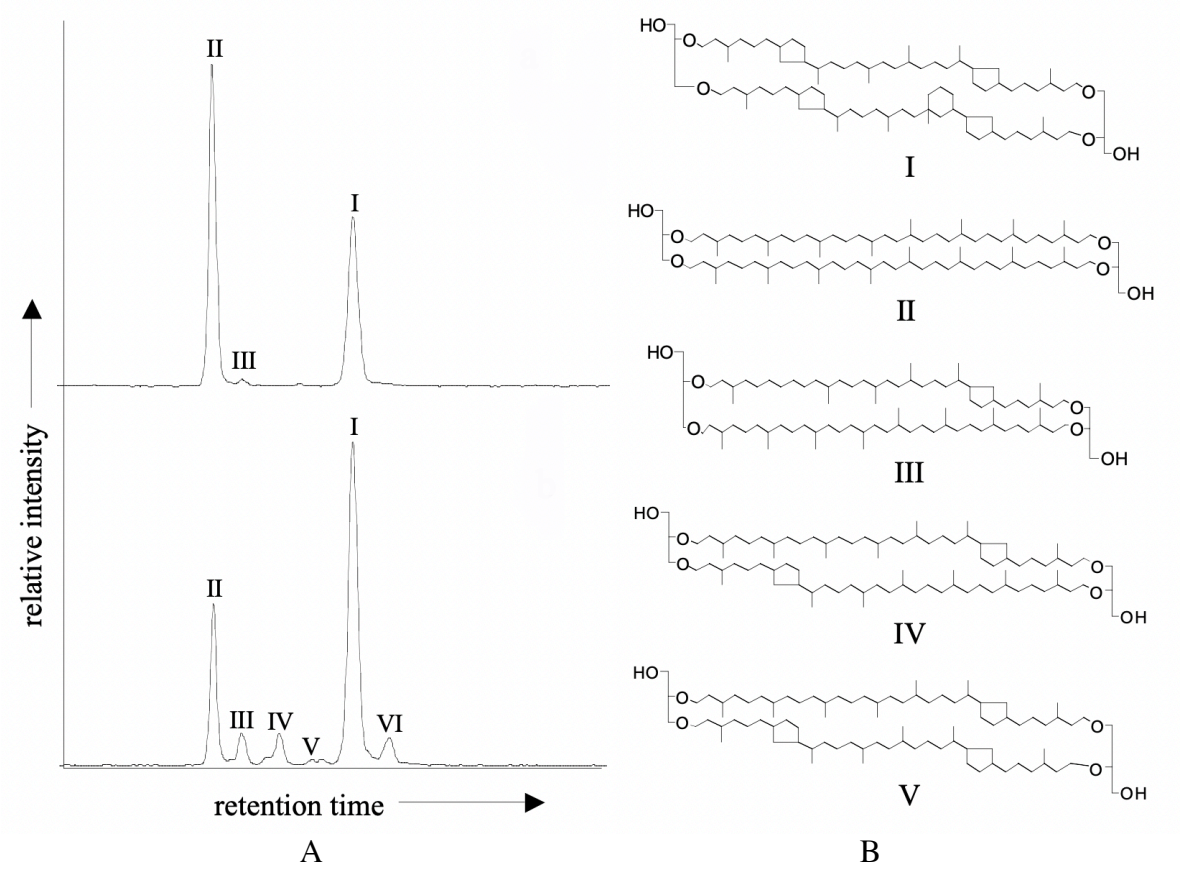

Fig. 1. A) Chromatogram of GDGTs. Top: shows Cold location with fewer rings of GDGTs detected in surface sediment from Halley Bay Station (Antarctica). Bottom: more GDGTs with rings are seen in a surface sediment from the Arabian Sea. (Arabian Sea). B) the molecular structure. Note: II, III, IV, and V refer to GDGT-0, GDGT-1, GDGT-2, and GDGT-3 while I refers to Crenarchaeol.

An initial study on the development of the TEX_{86} is that the average weight number of cyclopentane rings found in the surface sediment is calculated to quantitatively express the control of the temperature on GDGTs distribution and found that the TEX_{86} gave the best correlation.

$$TEX86 = \frac{([GDGT-2]+[GDGT-3]+[Cren'])}{([GDGT-1]+[GDGT-2]+[GDGT-3]+[Cren'])} \quad (1)$$

The correlation between this index and the annual mean sea surface temperature (SST) of the directly-overlying water gave a linear equation (*see equation (2)*) (Schouten et al., 2002).

$$TEX86 = 0.015 \times SST + 0.28 \ (r^2 = 0.92; n=44) \quad (2)$$

This relation was then improved using a more extensive, global core-top dataset (n=284) by Kim et al. (2008). An SST with a range of 5-30°C also exhibits a linear correlation (*see equation (3)*).

$$SST = 56.2 \times TEX_{86} - 10.8 \ (r^2 = 0.935; n = 223) \quad (3)$$

This study also indicated that the relationship was non-linear between -2 to 30°C, especially in the temperature range <5°C (Kim et al., 2008). In a subsequent study, the GDGTs distribution of a large number (116) of new core-top from non (sub)tropical oceans was analyzed further to improve the spatialcoverage of the core top dataset. Besides, satellite-derived SSTs were used instead of SST from the World Ocean Database (WOD) since it has a higher dataset resolution to determine the temperature signalof local sites near the shores (Kim et al., 2010). This study demonstrated the need for different calibration models for different temperature ranges; GDGT index-1 (TEX_{86}^{L}), without the crenarchaeol regio-isomer, is more relevant for cold oceans, whereas the GDGT index-2 (TEX_{86}^{H}) is more appropriate for (sub)tropical ocean SST determination. The different role of crenarchaeol regio-isomer in the different zones of oceans is likely because of the different relative abundance of this component in genetically distinct Crenarchaeota (Kim et al., 2010).

It is worth noting that the best combination of isoprenoid GDGTs now includes the crenarchaeol regio-isomer, which is exactly the same as the original TEX86 index (Schouten et al., 2002), but is now based on a logarithmic function (*see equation (4)*). Efforts to further improve the relationship are based on a comprehensive database (n=1095) and use a Bayesian regression approach, resulting in a calibration called BAYSPAR (Tierney and Tingley, 2014). From the TEX_{86} surface sediment database and extended Bayesian calibration, the SSTs derived from TEX_{86}^{H} were calculated with the temperature equations of Kim et al. (2010) based on the fractional abundances of GDGT-1, GDGT-2, GDGT-3, and the regio-isomer of crenarchaeol, Cren′. The TEX_{86}^{H} is related to SST using a global core-top calibration (Kim et al., 2010), excluding data from the (sub)polar oceans and the Red Sea with a calibration error at ±2.5°C.

$$TEX_{86}^{H} = log\ (TEX_{86}) \quad (4)$$

Despite these improvements, there is still some scatter and unexplained variation in the relationship between TEX_{86} and SST (Fig. 2). In addition to an uncertainty of the exact production depth (surface versus subsurface) and possible influence of seasonality, the TEX_{86}-based temperature estimate can be biased due to possible sources such as contributions from a deep-water community, methanogens, terrestrial input, and non-thermal co-founding effects of oxygen content or nutrient status. Specific indices, such as Ring Index, which can identify GDGT distributions impacted by non-temperature factors (Zhang et al., 2016), and the ratio between GDGTs bearing two vs three cyclopentyl moieties ([2]/[3] ratio) reflecting a contribution from Archaea living in the deeper water column (Taylor et al.,

2013), are all used to identify these potential overprints. However, after all these, there is still scatter remaining in the global core top dataset. Therefore, we investigate if lateral transport of GDGTs can explain the offsets between SSTs at surface water and the TEX_{86}-based SSTs.

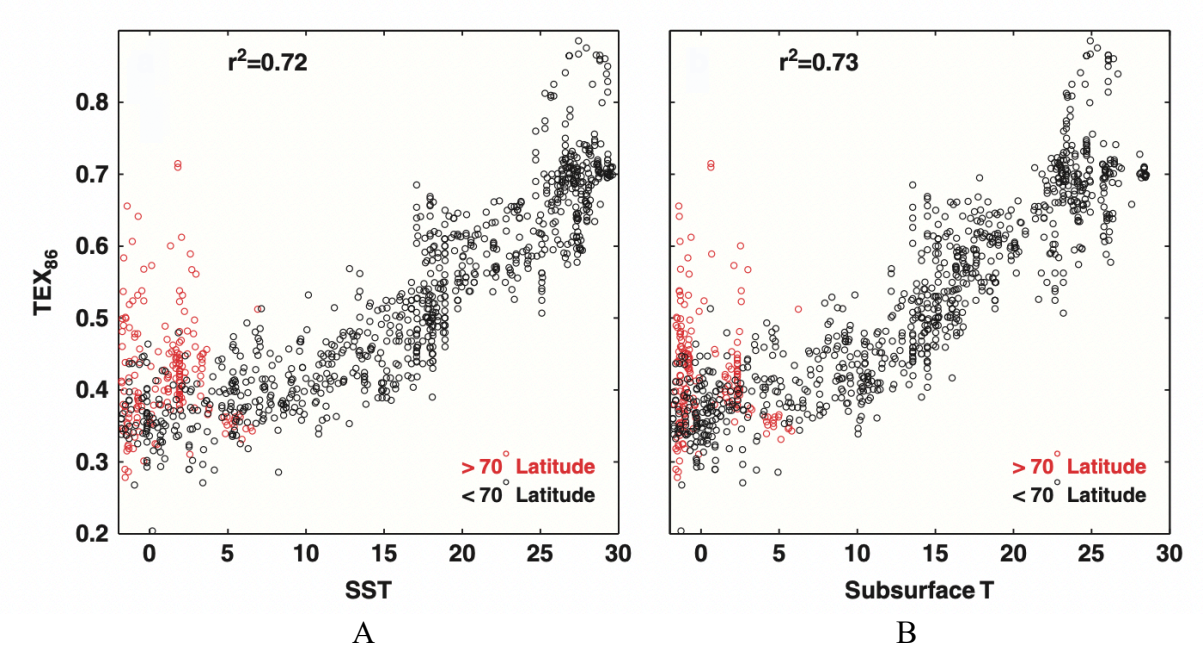

Fig. 2 The Scatter plot of the TEX_{86} database versus A) sea-surface temperature (SST), and B) subsurface (Sub-T; 0–200 meters. Red dots indicate data located above 70°N latitude; black dots show all other data. The TEX_{86} database confirms that the distribution of surface sediment GDGT has a strong relationship to temperature, accounting for over 70% of the variance in the data (Tierney & Tingley, 2015).

According to Trommer et al. (2009) and Ho et al. (2014), the relationship between TEX86 and temperature relationship seems different depending on ocean area and environment. Here, the underlying causes of scatter in the South Atlantic part of the TEX_{86}-SST calibration dataset were investigated, and the influence of lateral transport on the TEX_{86} signal during the sinking was identified. A sub-dataset of Subtropics was determined for a computational cost, and the South Atlantic was chosen due to the abundance of data and wide geographic spread, large spread of SST, and oceanographic regimes (polar versus tropical influence deep versus shallow settings).

As such, there are two scenarios in this study. Firstly, the GDGTs are produced in the water column and quickly transported to the bottom of the ocean. In this case, there is no correlation with lateral transport, meaning that it is just sinking vertically. Hence, the deeper the water column, the more contribution of GDGTs from organisms living in deeper water, indicating a possible overprint by a deep-water signal. According to Kim et al. (2015), the TEX_{86} value is not related to the water depth at deep water (> 1000 m) but reveals a strong correlation with annual average SSTs. Another aspect is that if the TEX_{86}-based SSTs in the sediment are not the same as SSTs on the overlying water, it must be lateral transport. However, that is not true because it can also be caused by another

factor. The offset between these two different SSTs can be a cold bias in regions under the influence of warm current. This is because TEX_{86}-based SSTs are lower than the directly-overlying SSTs. In contrast, a warm offset is in regions under the influence of cold currents. They specifically explain that an ocean model, fitted with a means to simulate sinking particles from the surface to the bottom, is able to check these scenarios.

Section 2 describes the study area, a compilation of the TEX_{86} and GDGTs data, and the methods for analyzing the transport of the particles. The first part of section 3 addresses the sources of scatter on the regional scale. The most dominant variables are defined by performing statistical analysis with a linear regression method. In the second part of the section, a subsequent analysis of the transport-related offsets is shown in three main specific regimes. Eventually, section 4 provides a conclusion.

2. METHODOLOGY

2.1 Study Area

The specific sub-dataset of core top TEX_{86} dataset (n=88), in the Subtropical South Atlantic Basin (23.5°S-40°S), was extracted from previous global calibration effort by Kim et al. (2010) and GDGTs distribution study in the South East Atlantic Ocean by Hernandez-Sanchez (2014) as a part of TEX_{86} surface sediment database with a BAYSPAR model approach by Tierney and Tingley (2014, 2015). Three clusters of the sub-dataset are then recognized with different depth ranges and prevailing ocean current (Fig. 3): The Southeast Atlantic (n=37; 20-5269 m), the South West Atlantic (n=35; 202-4512 m), and Central Gyre (n=16; 3525-4491 m).

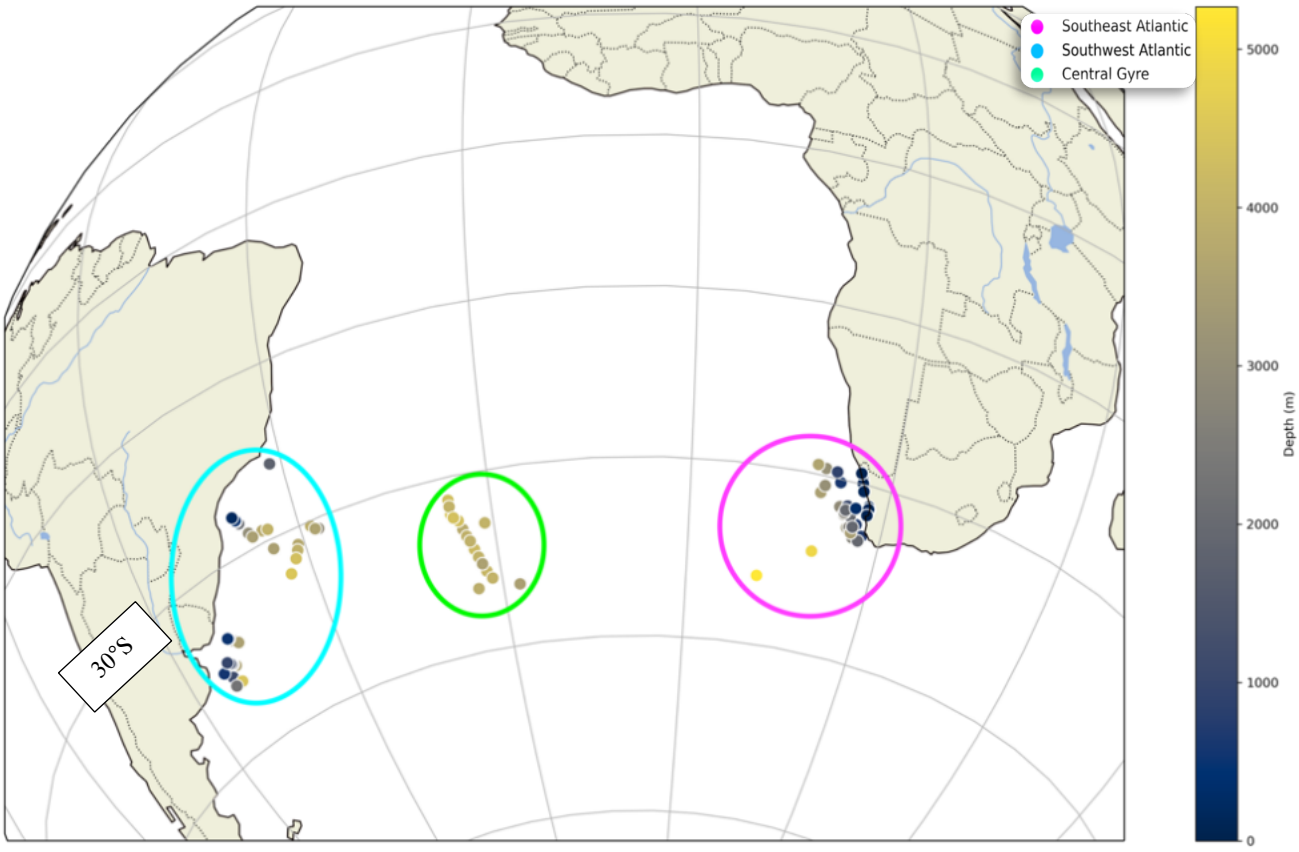

A

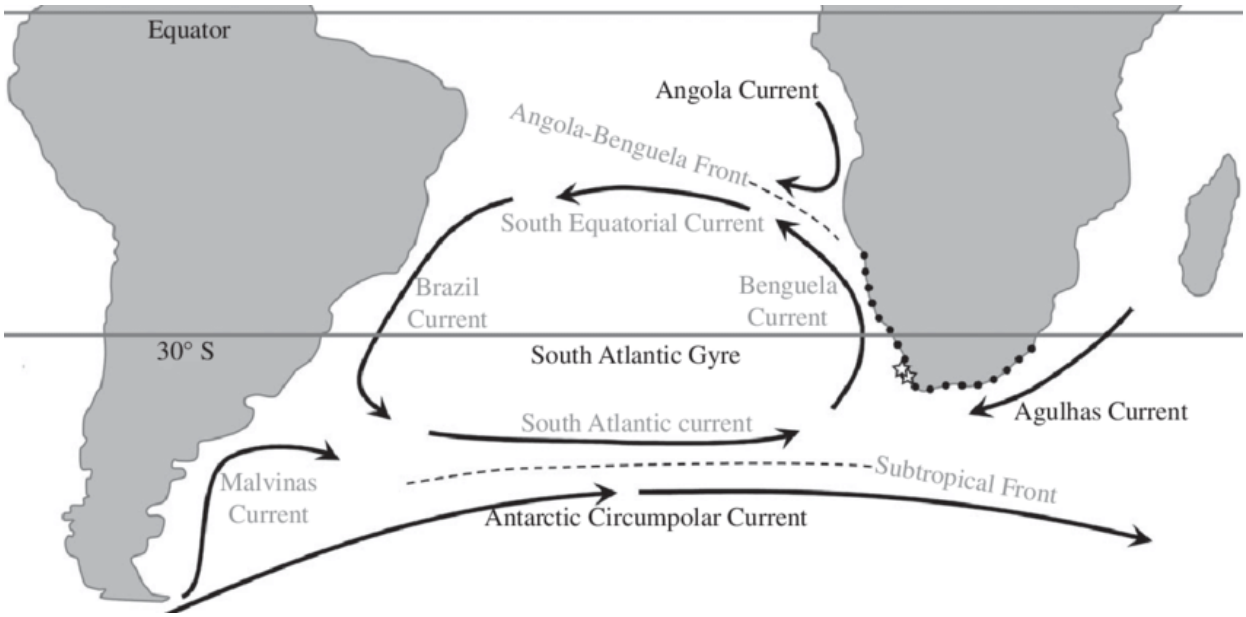

B

Fig. 3 A) The distribution of sedimentary core top data in the South Atlantic TEX86 sub-dataset. Three main clusters: the Southeast Atlantic (pink circle;7.670°E-18.222°E), the Southwest Atlantic (blue circle; 55.015°W-38.073°W), and the Central Gyre (green circle; 24.248). B) Surface currents in the South Atlantic Ocean (Ksepka and Thomas, 2011).

2.2 Compilation of the TEX_{86} and GDGTs Data

TEX_{86}-based SSTs and certain indices for assessing secondary effects are all computed based on the fractional abundance of GDGTs for each TEX_{86} site, including [2]/[3] ratio, and ΔRI. The exceptions are the lateral transport effect and depth. The depth values were already provided in the latest calibration (Tierney and Tingley, 2015).

2.2.1 TEX_{86}^{H}-based SSTs

To calculate SSTs, Kim et al. (2010) calibration is used (*see equation (5)*).

$$SSTs\ from\ TEX_{86}^{H} = 68.4\ x\ (TEX_{86}^{H}) + 38.6 \quad (5)$$

2.2.2 GDGTs Bearing Two vs. Three Cyclopentyl Moieties ([2]/[3] Ratio)

[2]/[3] ratio is a proxy for depth, reflecting a contribution from Archaea living in deeper waters. Sedimentary [2/3] ratios are usually lower in shallow settings in the modern surface sediment dataset. By extension, the application of GDGT-based temperature proxies may depend on depth. Shallow water settings will record surface water characteristic while deeper settings for a cooler temperature signal due to the greater contributions of GDGTs synthesized in the depths (Taylor et al., 2013).

2.2.3 ΔRI

The Ring Index is applied to differentiate the non-thermal factor-affected samples or those deviated from modern analogs (Zhang et al., 2016). The Ring Index (RI) is a weighted average of the number of the rings in the GDGT compounds, which also shows a strong relationship to temperature (*see equation (6)*).

$$RI = 0\times [GDGT-0] + 1\times [GDGT-1] + 2\times [GDGT-2] + 3\times [GDGT-3] + 4\times [Cren + Cren'] \quad (6)$$

In the modern dataset, RI is significantly linked (r^2 = 0.87; n = 531) to TEX_{86} (Zhang et al., 2016) expressed by quadratic regression (*see equation (7)*).

$$RI_{TEX} = -0.77(\pm 0.38) \times TEX_{86} + 3.32(\pm 0.34) \times (TEX_{86})^2 + 1.59(\pm 0.10) \quad (7)$$

Zhang et al. (2016) suggest that geological samples cannot confidently be used for palaeothermometry if they deviate from the modern TEX86-RI relationship (*see equation (8)*).

$$\Delta RI = RI_{TEX} - RI_{sample} \quad (8)$$

According to the 95% confidence interval (2σ) of the modern regression, > |0.3| value of ΔRI is considered to represent samples whose GDGT distributions reside outside the modern TEX86-RI relationship, reflecting the characters which are utterly different from the modern production of GDGTs (Zhang et al., 2016). With this approach, the Ring Index can determine samples affected by terrestrial inputs or methanotrophic archaeal communities and identify samples with atypical GDGT distributions probably impacted by non-thermal factors, e.g., Mediterranean Sea samples from < 1000 m water depth (Kim et al., 2015; Zhang et al., 2016).

2.2.3 Lateral Transport Effect with Particle Simulation

Lagrangian particle trace simulation (van Sebille et al., 2018) was used to quantitatively assess the biasing effect of the lateral transport of sedimentary particles in a high-resolution model on the South Atlantic sample locations in the TEX_{86} database. This simulator, called Parcels (Probably A Really Computationally Efficient Langrangian Simulator), contains a set of Python classes and methods Parcels (downloaded from github.com/OceanParcels/parcels), which enables to track both active and passive particulates released in Nucleus for European Modelling of the Ocean (NEMO; https://www.nemo-ocean.eu) flow field (0.1° horizontal resolution) with a five-daily output (*see Appendix A*).

The backward approach of Parcels, back-calculating the sinking trajectory from the sediment location to its origin at 30m water depth, was used. The particle tracking simulation could be employed on any sinking particle. For that reason, two slow-sinking speeds (10 and 25 meters/day) were set to propagate virtual particles, representing small and larger aggregates, respectively.

Indeed, deciding on a realistic sinking speed is complicated. However, these particles sinking velocities are determined based on previous calculations of 9-17 m/d near Cape Blanc and 25-27 m/d in the Arabian Sea based on seasonal SSTs of Sediment trap studies (Mollenhauer et al., 2015 and Wuchter et al., 2006, respectively). A study of ocean currents in sedimentary microplankton assemblages was also proposed by Nooteboom et al. (2019). This study reveals that the potential of these transportation effects can be implemented by a quick calculation. A dinocyst, for example, a particle which is also distributed by current, sinks into a depth of 4 km depth through the water column at 11 m/day (according to the standard of Anderson et al., 1985, for the sinking speed of the cysts), can reach the seabed after almost a year and could be displaced by up to 1,570 km from its surface location if the average horizontal ocean current velocity is about 5 cm/s. The sea surface locations where the GDGTs are produced were determined with the use of a physical ocean model NEMO, presenting a 3D flow field of the ocean currents.

In this study, the SSTs from the slow-sinking particles were subsequently compared to fast-sinking particles of 4000 m/d which represents the SSTs at directly overlying water. Here it is assumed that GDGTs in the surface waters are representative of those in sediments with a mechanism by which packaging of small GDGT-containing thaumarchaeotal cells into faecal pellets and 'marine snow' aggregates (Wuchter et al., 2005; Huguet et al., 2006), leading to the rapid transport of archaeal cells from the depth at which zooplankton graze to the seafloor (Huguet et al., 2006). The directly overlying SSTs were then compared to the modeled temperature after the transport effect is included.

The flow field for the fast-sinking particles to the bottom of the sea was determined, thus an offset called ΔSST (*see equation (9)*). The model resolution sets a maximum offset of 15 km between sediment location and overlying water location. The sinking speed scenarios-based temperatures from the model were chosen rather than those from World Ocean Atlas 2009 (WOA09) on the calibration to avoid complications due to differences in the two datasets. First, modeled SSTs are probably more appropriate than the WOA SSTs since model-to-model SSTs are compared, although WOA09 SST is also valid for 2009 during which SSTs based on the fast-sinking particles were set. Second, The NEMO model is linked to a biogeochemical model and provides more environmental variables such as salinity. Lastly, the difference between the SST_{TEX86} and modeled-overlying SST becomes much more significant and seems complicated when WOA09 SSTs are used (*see Appendix B. 1*).

Another term is ΔSST bias, referred to as an offset between SST_{TEX86} and SSTs at directly overlying water with lateral transport effect, which is the average SST of the surface locations of the backtracked particles of that sediment location (*see equation (10)*). The lateral transport-related SSTs were defined using a modeled SST with both 10 m/d and 25 m/d sinking speed scenarios. These two different velocities were used to explain whether lateral transports of the particles influence on the relationship between TEX_{86} and temperature in the region and to show if there is a difference it makes. In short, this terminology is used to distinguish it from the offset without the transport effect.

ΔSST = the TEX_{86}-derived SST (SST_{TEX86}) – modeled-overlying SST (9)

ΔSST bias = SST_{TEX86} – modeled average SST of transported particles (10)

For All possible overprints and deviations, Linear Regression Method was used to assess whether it applies to the dataset. Pearson Coefficient (*see Appendix C*) and p-value were calculated to see which variables are dominant towards ΔSST bias.

3. RESULT

First, a magnitude of lateral transport influence in the South Atlantic Ocean and the sources of scatter are analyzed on the regional scale. The region is then divided into three different clusters to do a subsequent analysis of lateral transport-related offsets in this sub-basin.

3.1 The Influence of Lateral Transport on the Temperature Relation of TEX_{86} in the South Atlantic Ocean

The lateral transport was firstly investigated by showing the deviation and the correlation and found that this is true for the complete Subtropical South Atlantic Ocean sub-dataset. In general, there is not much difference between ΔSST (4000 m/d) and ΔSST bias (10 m/d). The most obvious is that there is a slight shift towards positive values of the offset (ΔSST) when considering lateral transport (ΔSST bias) even though the mean decreases, declining from -0.22 and -0.39. This is because there a strong influence of lateral transport, indicated by the largest cold offset of -10°C (Fig. 4A). The standard deviation of the offset is to increase, raising from 2.89 to 3.24. The r-value of offset is relatively smaller for the entire dataset if lateral transport is considered, slightly decreasing from 0.76 to 0.66 while p-values are all < 0.05 (Fig. 4B).

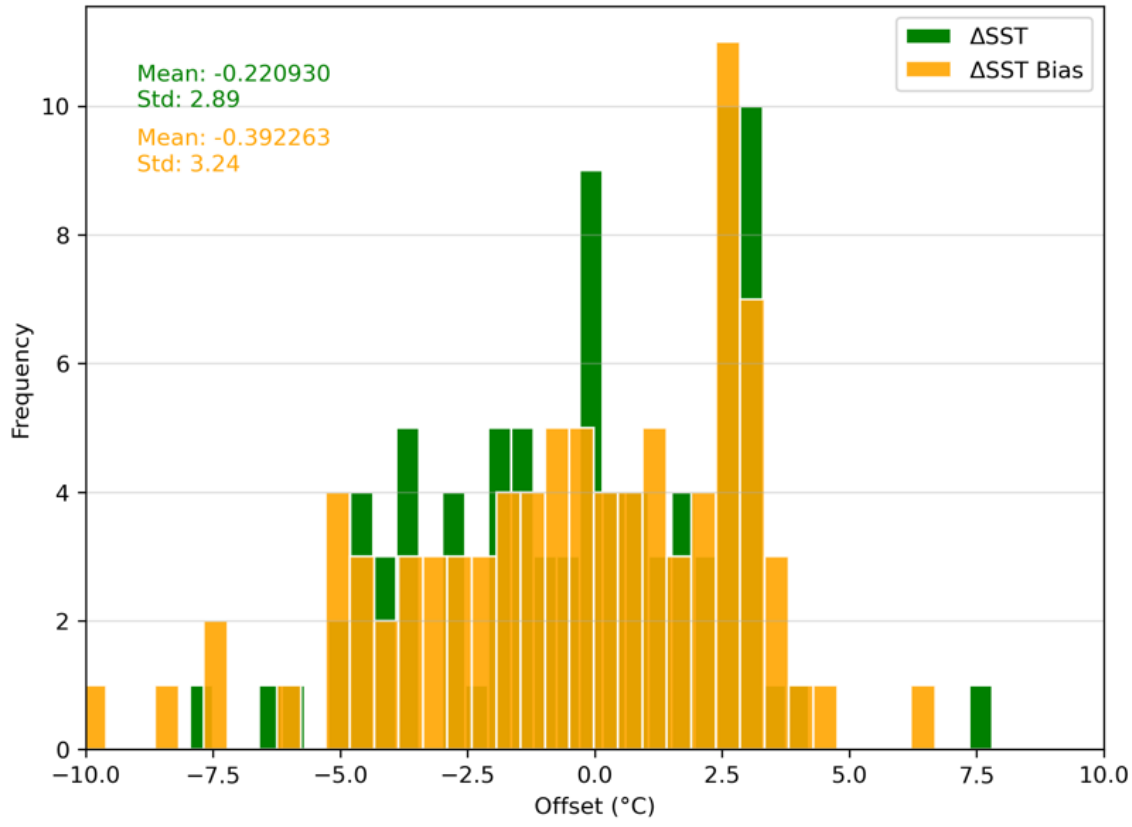

A

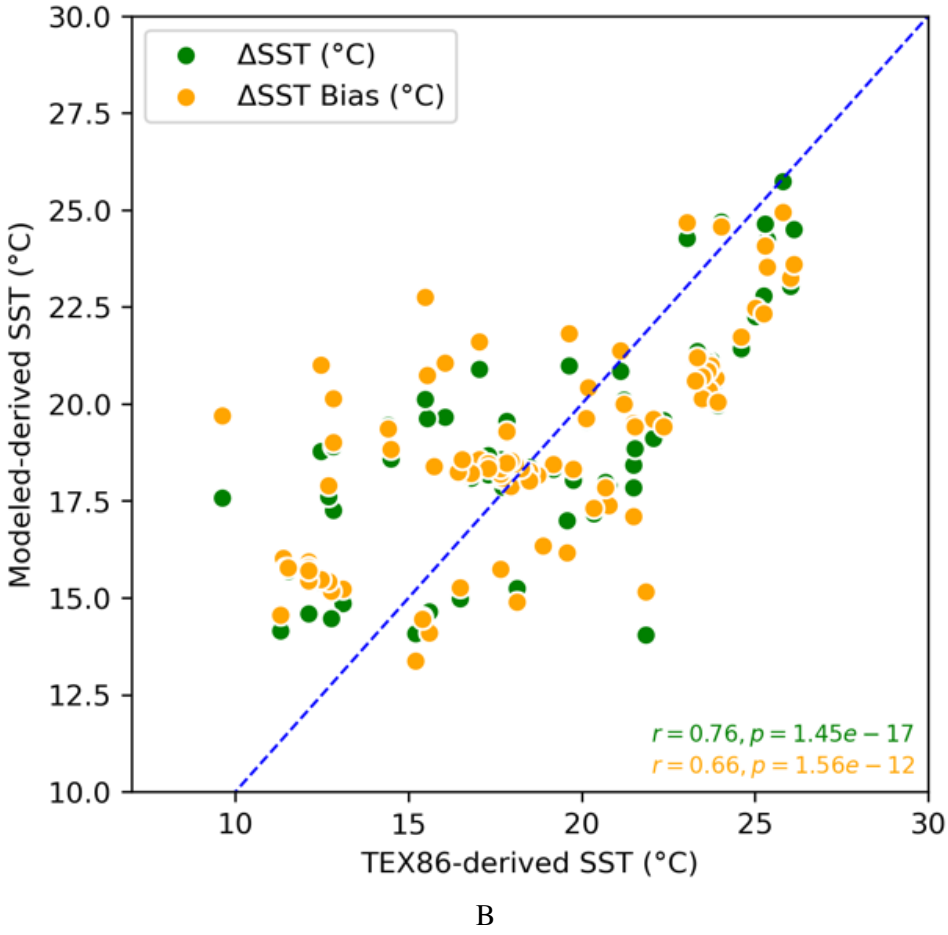

B

Fig. 4 The offset comparison between ΔSST and ΔSST bias. The Normal distribution is given in A (the green bar represents ΔSST, derived from the TEX_{86}-derived SST (SST_{TEX86}) – modeled-overlying SST), and the orange bar represent ΔSST Bias, derived from SST_{TEX86}) – modeled average SST of transported particles). The difference between ΔSST and ΔSST Bias is highlighted in B, exhibiting a strong relation by using Pearson Correlation Coefficient (ΔSST:0.76; ΔSST Bias:0.66). Note: 4000 m/d is used in ΔSST while ΔSST bias is at 10 m/d sinking speed.

The SSTs of the directly overlying water hardly differ from those of the average of transported particles, which suggests that lateral transport does not explain a large part of the scatter in the core-top sub-dataset. It is expected that if lateral transport would have a large effect, samples from ΔSST bias would move closer to the 1:1 line (Fig. 4B). Indeed, there has been a difference between the TEX_{86}-derived SSTs and the directly-overlying SSTs without considering the lateral transport. This means that there has been an offset between the temperatures starting off sinking and those arriving at the sediment due to other factors which determine most of the scatter in the core-top dataset.

The most significant negative deviation due to lateral transport ranges from -5 °C to -10°C, indicated by the darker blue scatters in the Southwest Atlantic (Fig. 5A). Surprisingly, most of these sites in the core top dataset are relatively close to the coast and hence in relatively shallow basins. The sites with a negative ΔSST bias are considered the samples where lateral transport occur because these are only visible when both the ΔSST and ΔSST bias are negatively deviated (Fig. 5B). Since the bias can be

seen from the scatter deviated from the one-to-one line, it is plausible to conclude that changing the sinking velocity assumption for the particles at 10 m/d (indicated by orange scatters) or 25 m/d (indicated by red scatters) will only affect the magnitude of the bias, not the geographical structure of where the lateral transport is essential (Fig. 5B). Of course, the sinking speed assumption does influence the magnitude of the lateral transport distance of the particles and, therefore, the magnitude of the potential bias; however, the values are not significantly different. One upper extreme value is also observed: i.e. lateral transport of the particles in deep basin takes place in the core top D357 St at 5263 m – the maximum recorded, in the Southeast Atlantic.

Interestingly, the bulk of the sub-dataset is within calibration error at ± 2,5°C for the global TEX_{86} dataset by Kim et al. (2010), at 39,6% and 36,9% of the total sample for ΔSST and ΔSST bias, indicated by the Interquartile range (IR). Moreover, the mean of the offset in the sub-dataset is also almost the same as that in the global dataset (± 0°) (Fig. 4B).

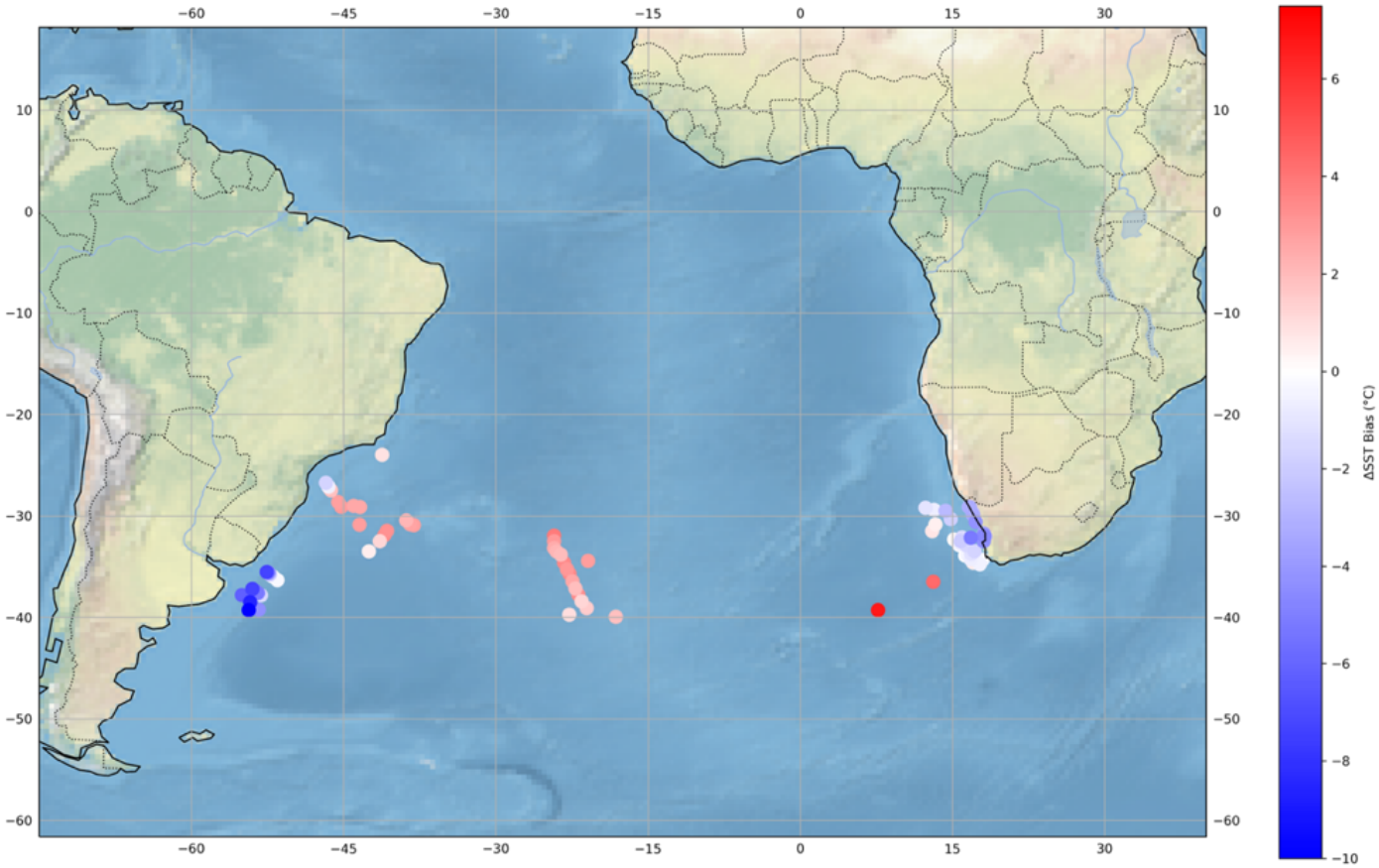

A

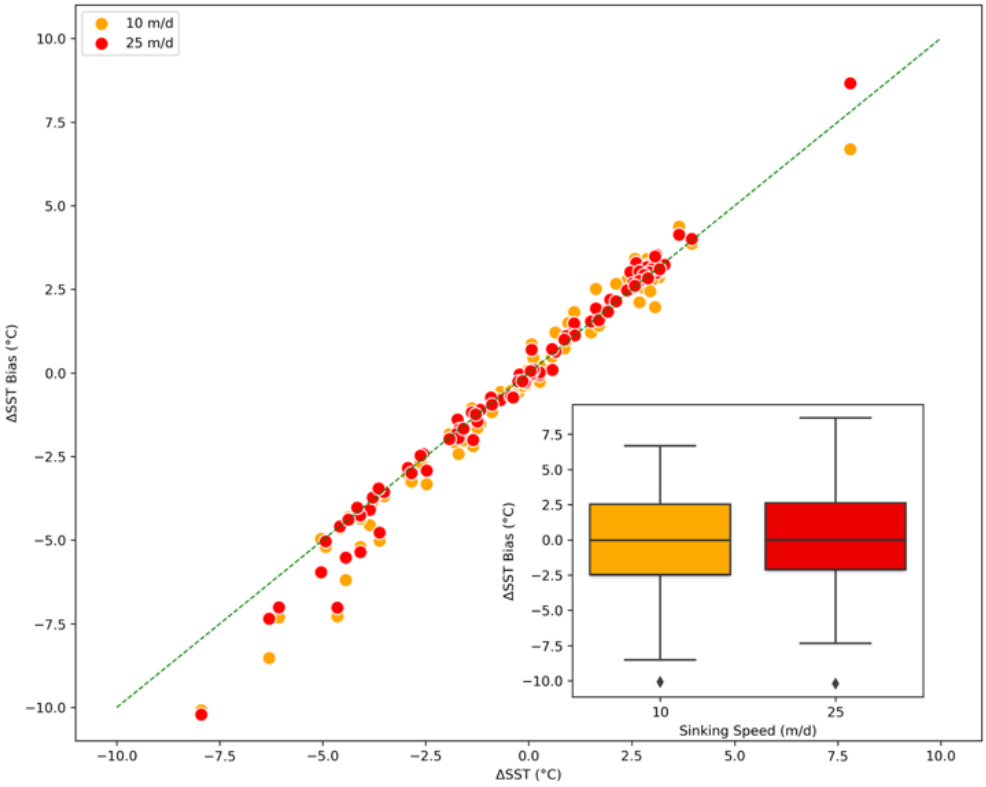

B

Fig. 5 A). The Distribution of ΔSST bias (10 m/d) on sedimentary core top data in the South Atlantic TEX_{86} Database. B) The relationship between ΔSST and its bias due to lateral transport with two different sinking speeds (10 m/d and 25 m/d). The insert indicates fewer extreme values of ΔSST bias.

For completeness, the results for the subsurface (150 m water depth) is also presented (see Appendix B. 2). Crucially, this confirms that the choice of the depth (30 m or 150 m) where the particles start sinking does not influence the scatter deviation or the fact that the subsurface temperature parallel with SST, and thus does not change our conclusion regarding the lateral transport.

3.2 Identifying the Sources of Scatter

To investigate any potential secondary controls on the TEX_{86}, the sources of scatter such as lateral transport and depth along with a variety of GDGT distribution parameters ([2]/[3] ratio, and ΔRI) were assessed. These parameters were then compared to the horizontal travel distance to see if the control of lateral transport of sinking particles can be relevant in the Subtropical South Atlantic Ocean basin,

It was observed that depth and [2]/[3] ratio are important explaining variables for the scatter in the core top sub-dataset in the South Atlantic, indicated by a strong and statistically significant correlation to ΔSST bias (6C: r=0.71, p=1.42e-14; and 6B: r=0.70, p=2.74e-14*)*. However, ΔRI shows a negatively weak correlation (-0.39), and there is no significant correlation between the lateral transport and TEX86 (r=-0.12, *p*=0.26).

Numerous sites where the particles were not transported far (< 200 km) have relatively substantial cold ΔSST bias (up to -10 °C). According to depth, ΔSST bias is negatively ranged in epipelagic zone (<200 m), whereas the highest positive offset (6.68 °C) is detected in the deepest site (the South East Atlantic; 5269 m) (Fig. 6B). Unusually, SSTs derived from GDGTs in sediments from the epipelagic zone have a cold offset given there should not be much lateral transport due to the relatively short sinking time for the particles at shallow sites (0-200m water depth). Additionally, it is expected that ΔSST bias is hovering around 0. On the contrary, all of the data have a consistent cold offset, and deeper sites consistently a have warmer bias on more samples. In fact, all sites in epipelagic and mesopelagic (<1000 m) also show negative value at ΔSST (*see Appendix B. 4*), showing a depth difference between ΔSST and ΔSST bias.

Similarly, the sites with a positive offset have high [2]/[3] ratios, suggesting an explicit attribute of deep community overprint. It is reasonable because the depth and [2]/[3] ratio is strongly correlated as [2]/[3] ratio is used as a proxy for deep water community distribution.

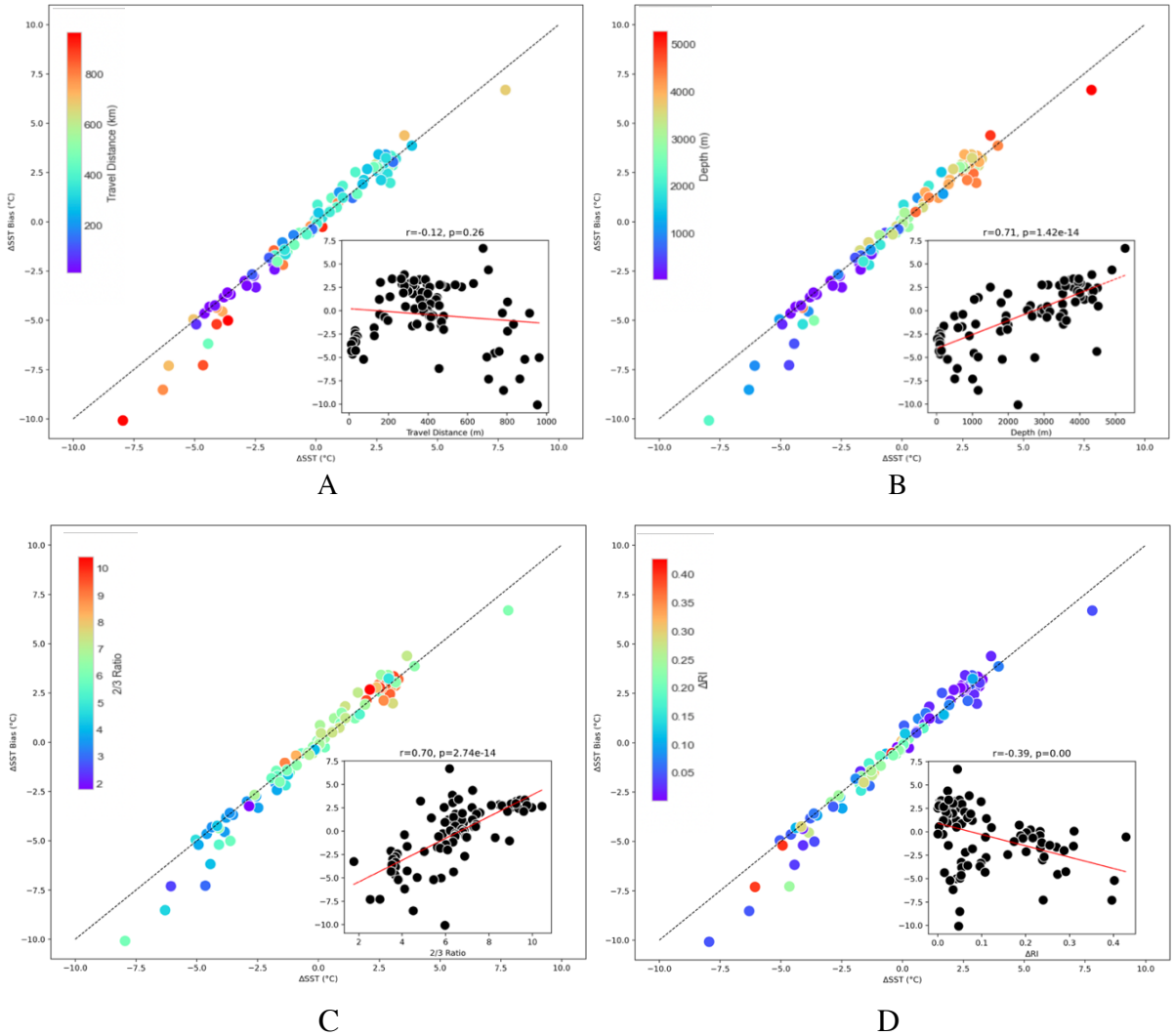

Fig. 6 The correlation of ΔSST Bias due to lateral transport over four possible sources in the South Atlantic Ocean. A) Travel Distance. B) Depth. C) [2]/[3] Ratio. D) ΔRI.

Based on the explanation above, there is an apparent change of ΔSST and ΔSST bias with depth. The deeper the water column, the more time is needed to transport and more time to be influenced by water contribution, assuming that ΔSST bias is invariable with the depth. Thus, there is more lateral transport in deeper sites. However, it would also mean that there is more time for this deep-water contribution to add to TEX_{86} signal. These forces make the calibration underestimate TEX_{86} in shallow waters and overestimate TEX_{86} in deeper waters. Consequently, water depth exerts a larger control on the TEX_{86} in comparison to the other parameters.

It is also interesting to note that ΔRI < 0.10 considerably dominates whereas a few samples show higher numbers at > 0.30, suggesting a significant deviation from modern analogs and/or a strong influence from non-thermal factors. The highest number is indicated by cold ΔSST (around 5 °C), similar to the ΔSST due to the lateral transport bias.

3.3 Biasing Effect of Ocean Current Versus Other Three Possible Sources of Scatter in Different Oceanographic Settings

In the subsequent section, the sub-dataset is divided into three main Clusters: The Southeast Atlantic, the Southwest Atlantic, and the Central Gyre (Fig. 3). These three places are under entirely different current regimes although they are located in the same gyre system.

From the regional simulation, the locations where lateral transport is the most explaining variable can be identified since a large part of the South Atlantic Ocean is under gyre system, thus different specific local ocean currents. The amount of lateral transport of sinking particles was studied to see if it can be relevant by statistically clustering the Subtropical South Atlantic Ocean dataset into three clusters. First of all, an opposite relationship between the Southeast Atlantic and the Southwest Atlantic was observed.

Similar to the regional scale, the depth dominated on ΔSST bias compared to the other possible sources of scatter in the Southeast Atlantic, showing a high positive relation (r=0.85), followed by [2]/[3] ratio indicating the presence (and overprint) of a deep water community on the TEX86 signal produced in the (sub)surface (r=0.62). Suprisingly, lateral transport also shows a strong influence, standing at 0.83 to be precise. The exception is delta RI, as its p-value is greater than the significance level (0.32) (Fig. 7).

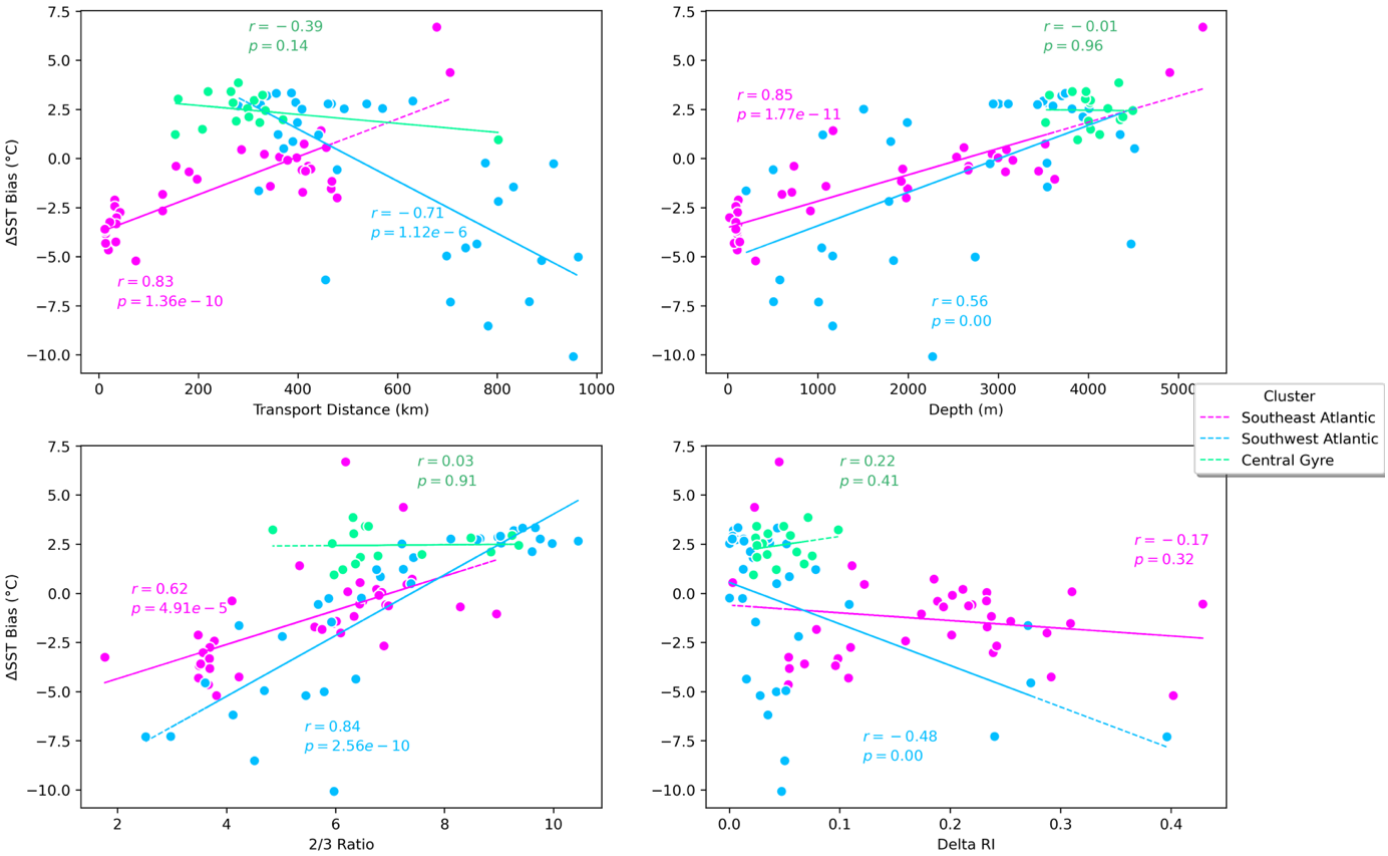

Fig. 7 The correlation of ΔSST Bias due to lateral transport over four possible Sources A) Travel Distance; B) Depth; C) [2]/[3] Ratio; D) ΔRI, in three main region: Southeast Atlantic (Pink dot), Southwest Atlantic (Blue dot), and Central Gyre (Green dot).

The depth range of both sides is much broader than that in the Central Gyre since the coastal samples of both are also included, whereas the samples in the central gyre are deep everywhere at >3000 m (Fig. 7B). More interestingly, the Southeast Atlantic exhibits a positive correlation with lateral transport. The larger the distance, the larger ΔSST deviation, contrasts with what happened in the Southwest Atlantic where the ΔSST bias becomes more negative as distance increases (Fig. 7A).

Still, a presence of deep water community was detected to have an influence on TEX86 or the SST signal, indicated by a high [2]/[3] ratio which significantly outnumbered the other variables in the Southwest Atlantic (r-value >0.80), while lateral transport is slightly lower at -0.71. Depth and ΔRI here only show a moderate correlation, standing at 0.56 and -0.48, respectively (Fig. 7). The negative relation between lateral transport and ΔSST bias in the Southwest Atlantic implies that ΔSST bias decreases with an upward distance. ΔSST bias becomes colder where the particles coming from the areas. This is because lateral transport-related SSTs are lower than TEX_{86}-derived SST.

Compared to other clusters, the Central Gyre does not really show a diagonal line in all variables, and the p-values are all more than significant level, indicating that there is insufficient evidence in the

sample to conclude that a non-zero correlation exists (Fig. 7). Moreover, it is clear that there is an overestimation of ΔSST bias, denoted by positive offset even though ΔSST also exhibits overestimated offset (see Appendix B. 5). Furthermore, the water depth ranges from approximately 3500m-4500m, which does not imply that there is no lateral transport influence there; The travel distance is always equally significant at <400 km, except for one site (802,1 km). Logically, the water entering the basin in the middle of the gyre does not flow fast so that there is much less lateral transport to begin there. Notwithstanding, [2]/[3] ratio is high (5-9), which is anomalous. This result behaves differently from the other clusters due to varying wide range – especially in the Southeast Atlantic, where some of the sites are deeper than the Central gyre, resulting in higher [2]/[3] ratio values. Hence, this was not seen much in the Central Gyre sample set because there is not much variability, indicated by the straight line (Fig. 7C).

3.4 Case Model of Particle Backtracking of the Core Top Sediment

Our analysis of ΔSST bias-travel distance correlation, coupled with depth range, leads us to reassess the controls of lateral transport on the offset. In this part, the travel distance against the ΔSST bias with the different water depths are displayed.

Our simulation shows that the larger the travel distance, the more significant the offset. Of course, cold and warm bias is related to depth, and it seems that in shallow sites, there is an underestimation of ΔSST. It is valid particularly for all sites except a few sites situated at Epipelagic and Mesopelagic zones (0-200m; 200-1000 m depth; herein categorized as “shallow”), yet they still have traveled far (up to almost 1000 km). These observations support the idea that the depth of the water column is not the primary control of the travel distance of the particles, but substantial local currents can contribute to this. It is important to note that if the distance is far but if the temperature is not changed, there is no transport influence on TEX_{86}-based SST; i.e, two sites in the Southwest Atlantic (Fig. 8A)

The longest distance for each cluster is shown by the circle points (The Southeast Atlantic: 408,9 km at 712 m depth; The Southwest Atlantic: 864,5 km at 508 m depth). The triangle ones, however, are sites located at deep water (>1000 m) where the particles were transported the furthest, representing each cluster (the Southeast Atlantic: 705,6 km at 4900 m depth; the Southwest Atlantic: 962,7 km at 2743 m; the Central Gyre: 802,1 km at 3878 m depth) (Fig. 8).

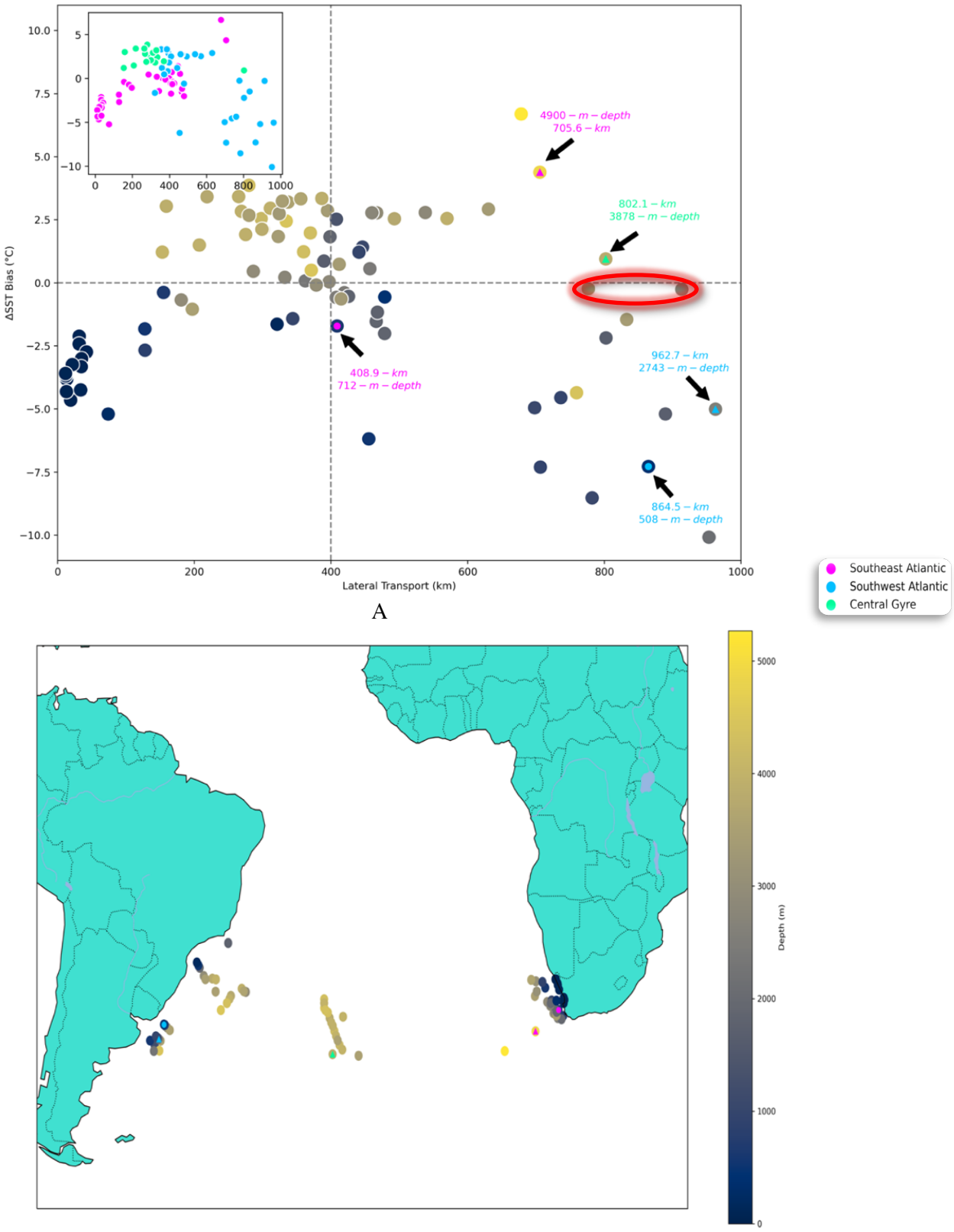

Fig. 8 A) Particles' distribution for three different oceanographic settings, exhibiting different magnitude of SST bias and travel distance. Overall, starting from 1000 m depth, the transport becomes more than 800 km. However, in the very deep site, the transport is decreased (but still large). Red circle indicates two sites which are not influenced by lateral transport, even though the particles were far transported (b) Map view shows geographically difference. the circle points represent the shallow sites (<1000m) while the triangle points represent the deep sites, representing the highest travel distance. Pink, blue, and green successively denotes the Southeast Atlantic, the Southwest Atlantic and the Central Gyre. Note: The shallower sites are 18 in total (The South East Atlantic:14 out of 37 in; the South West Atlantic: 4 out of 35; Central Gyre: 0 out of 16).

In order to see the particles' trajectory and prevailing ocean current, the trajectory simulation with oceanographical difference among the clusters were performed. The simulation includes the shallow and deep settings with the highest travel distance, informing the origin locations where the particles arise and the specific current that has transported them. The points with the furthest travel distance both in shallow and deep water are visible, and prevailing currents seem to control the particle's distribution (Fig. 9).

Overall, the particles' trajectory in the deep sites appears more complicated with a further travel distance, and the faster sinking speed seems to be more representative of the biasing effect of ocean current (Fig. 9B). It is very complicated since ocean currents do not flow in a straight line with many turbulent eddies over the South Atlantic. The Southeast Atlantic is subjected to Agulhas Current while the Southwest Atlantic is influenced by two currents: the Malvinas Current from the Southern Ocean and the Brazil Current from the Equatorial Current.

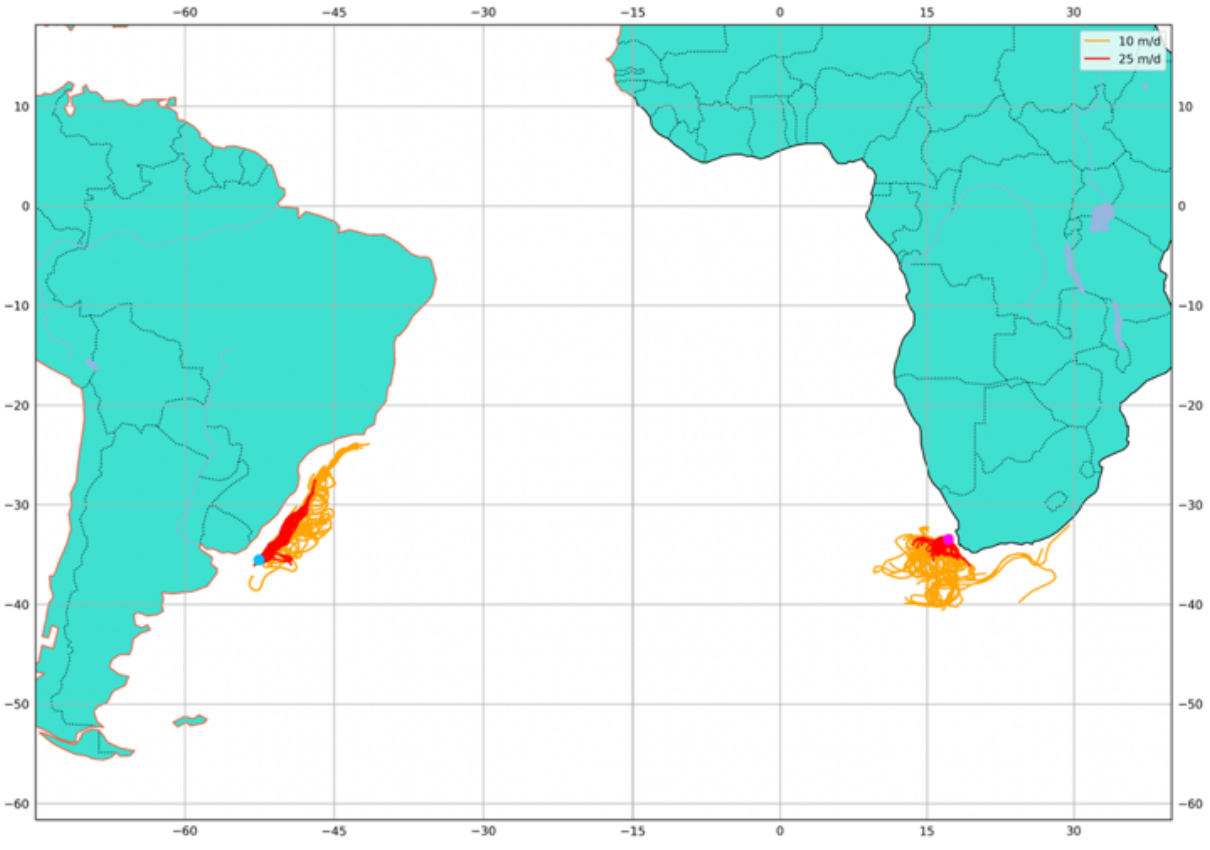

A

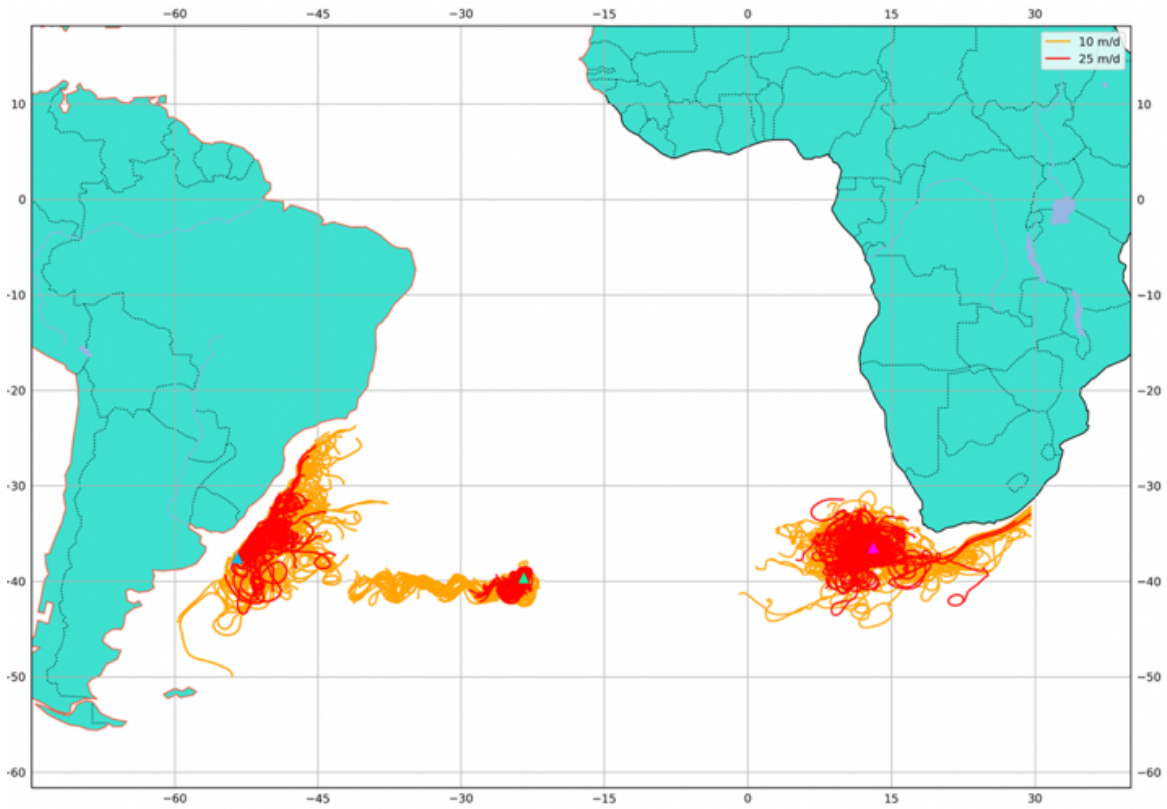

Fig. 9 Example of the particle backtracking for core top sediment. Regional variations of the effects of lateral transport during sinking of each cluster, representing the highest travel distance to see an improved relation between the particle occurrence and sea surface conditions. A) Shallow sites (<1000m) B) Deep sites (>1000 m).

DISCUSSION

The result from the statistical analysis of the travel distance of the GDGTs-bearing particles at Subtropical South Atlantic Ocean supports the expected hypothesis. The findings showed that lateral transport also plays a role in the scatter of the TEX_{86} calibration, yielding a larger offset. Ideally, there is no difference between the directly overlying water temperature and those in the sediment sample point (offset=0) unless there are processes taking place during the sinking, resulting in the increasing difference. Accordingly, it is entirely logical to consider lateral transport as a secondary control given that it also increases the scatter in the calibrations in the total dataset (South Atlantic sub-basin). Still, other factors than lateral transport determine most of the scatter in the core-top sub-dataset. This finding is similar with study done in the Southern Ocean by Kim et al. (2009) that from the TEX86 is dominantly affected by local conditions and less subjected to long-distance lateral transport.

Our finding also showed that changing the sinking velocity assumption for the particles (10 m/d or 25 m/d) will not affect the geographical structure of where the lateral transport is essential, but only the magnitude of the potential bias which are not significantly different. The increasing magnitude of the biasing effect of lateral transport with sinking speed scenario is also showed in recent study of

dinoflagellate by Nooteboom et al (2019). This study demonstrated that locally, at higher sinking speeds, the travel distance is still very large. If the sinking speed is close to infinity, it becomes 0. Most of sites in the core top data set (Zonneveld et al., 2013a) are relatively close to the coast and hence in relatively shallow regions. As a result, compared to the global average ocean, the particle transport at the sample site locations is on average lower.

It was also found that the choice of SST or the subsurface temperature does not change our conclusion regarding the lateral transport. This is surprising since it is in contrast with previous studies that a subsurface GDGT export is a common phenomenon, and TEX_{86} values shown in many regions seems to reflect thermocline instead of surface temperature, reported in the Benguela upwelling system (Lee et al., 2008), the northeastern tropical Atlantic (Lopes dos Santos et al., 2010), the tropical Pacific Ocean (Ho et al., 2011) and off the coast of Antarctica (Kim et al., 2012a). The latest paper by Ho and Laepple (2016) also supported the idea, proposing that the deposited GDGT came from the thermocline (TEX_{86} reflects the subsurface temperature, not SST). Nonetheless, their conclusions remain controversial due to the inconsistent assumption with all modern and microbiological evidence (Tierney et al., 2017). Schouten et al. (2013) suggested that if subsurface GDGTs are exported to the sediment, this may not influence the reability TEX_{86} as surface and subsurface temperature, which are closely coupled proxy. Other calibration efforts have attempted to calibrate integrated shallow subsurface (0–200 m) temperatures (as opposed to SSTs) – to the deposition GDGT distributions (Kim et al., 2012a, b). However, most work assumed that there is no deep (200 m) subsurface effect (Taylor, et al., 2013; Tierney and Tingley, 2015). Taylor, et al. (2013) also suggested that the effect is less for TEX_{86}^{H} and for TEX_{86}^{L}, but it is not absent and proposed a way to detect influence from subsurface GDGTs with the GDGT [2]/[3] ratio as a proxy for deep-water Thaumarchaeota influence with different GDGT distribution characteristics.

A positive offset have high [2]/[3] ratios in the result suggests that there is an explicit attribute of deep community overprint. It is reasonable because the depth and [2]/[3] ratio is strongly correlated as [2]/[3] ratio is used as a proxy for a contribution from deep water communities. These communities also produce GDGTs with a different 2/3 ratio, influencing the TEX86 signal. The differences in GDGT distributions with depth could reflect variations solely within the thaumarchaeotal community, also reported in previous experiments (Massana et al.,2000, Mincer et al., 2007). Additional evidence for different deep and shallow water communities (in the South China Sea) was reported by analyzing of the 16S rRNA genes, amoA gene, and biotin carboxylase gene accA, which may be related to the CO_2 fixation of archaea (Hu et al., 2011a,b). Therefore, it is likely that a part of this deep-water thaumarchaeotal community has a very high [2]/[3] ratio, incorporated into sinking material, and contributes to the sedimentary GDGT distribution. A potential print was also observed in the modern Mediterranean Sea, and Portuguese continental margin sediments influence can also be indicated by

increased proportions of the crenarchaeol regio-isomer (Kim et al., 2015; Kim et al., 2016). It is also worth to note that the TEX_{86}^{H} value is not related to the water depth at deep water (> 1000 m) but reveals a strong correlation with annual average SSTs (according to Kim et al. (2015). Phylogenetic analyses showed that the Thaumarchaeota communities identified at water depths of 1 m and 50 m are different from those at 200 m and 1000 m water depth, indicating high surface-sediment TEX_{86}^{H} values possibly because of the deep-water population of Thaumarchaeota. These studies showed that (1) under certain settings, TEX_{86}^{H} value is controlled by water depth and other TEX-based indices (Taylor et al., 2013; Kim et al., 2015; Kim et al., 2016). This is possibly due to the effect of deep-water Thaumarchaeotal communities on sedimentary isoGDGT distributions (Kim et al., 2016), and (2) a statistically different TEX_{86}^{H}-temperature correlation from the general global correlation in some water depth setting (> 1000 m) (Kim et al., 2015).

The influences on TEX86 besides temperature are stronger in the South Atlantic sub-dataset compared to the global dataset. This is probably because the sub-dataset covers a smaller temperature range (Regional: 13.4 °C – 24.9 °C; Global: -1.8°C to 29.6°C), while the full depth range of the global dataset is covered in the sub-dataset. Hence, the depth becomes more critical in explaining variable as a secondary influence in this basin.

What governs the different offset In the Southwest Atlantic throughout the water column is likely related to warm water brought by the Brazil Current. This result is in good agreement with the findings that SST behavior detected in The Brazil Current brings warm subtropical water while the Bengeula Current forms the east side of the subtropical circulation of the South Atlantic Ocean, transporting a mixture of relatively fresh and cool Atlantic water and relatively warm and salty Indian Ocean northward (Majumder and Schmid, 2017; Pierini et al., (2016). This opposite correlation indicates that there are two processes taking place due to lateral transport.

Notably, lateral transport influence is visible after dividing the basin. It is less important on the regional scale because positive and negative ΔSST bias compensate each other in all sub-dataset, but it is clearly shown in front of South America and Africa. Indeed, deep water community become the major influences on these regions. Similarly, the travel distance employs a primary effect to ΔSST bias, influenced by different ocean currents depending on the side of the basin. This is against the result in the regional scale that all of ΔSST bias is due to [2]/[3] ratio, and most likely that both travel distance and ΔSST bias are related to water depth. It may also be a cofounding effect of [2]/[3] ratio with the lateral transport, and the effect seems to override the [2]/[3] ratio despite the idea of [2]/[3] ratio affecting the TEX_{86}. Both the Southeast Atlantic and the Southwest Atlantic are generally well correlated with water depth, travel distance, and [2]/[3] ratio, whereas the scatter appear to be different in the Central Gyre.

The trajectory simulation exhibits that in addition to water flowing on the East Coast of the South American Continent, there is also a current coming from the Southern Ocean. This observation is similar to a study done by Matano et al., (2010) that there is a proportion of the particles that comes from Drake passage from the Antarctic peninsula. They add that even though there is only a smaller number of more extreme particles, the Antarctic Circumpolar Current (ACC) has a robust upward trajectory following the bathymetry at the Southern tip of Argentina. It then goes northward impermanently before flashing off, leading to eddies floating off the Antarctic circumpolar current, bringing the particles far to the north. Temperature and salinity are locally observed at the Uruguayan Margin (the Southeast of Brazil), where the Malvinas current (from ACC) and Brazil current meet. Hence, this can be an explanation for the underestimation of ΔSST bias in this region due to lateral transport itself.

Implication

As an investigation of how the GDGT-bearing particle distribution in surface water relates to the GDGT signals preserved in sediments, our experiment in the South Atlantic Ocean provides a new insight into the relationship between the TEX_{86} and the lateral transport as one of secondary controls on the scatter. However, the sub-dataset highlights several important 'gaps' which need to be filled to significantly improve understanding of GDGTs distribution. Therefore, we suggest screening sedimentary GDGT distributions for other potential secondary influences on TEX_{86} by utilizing some proposed and/or established GDGT indices: the BIT index which can identify if there is an input of soil-derived isoGDGTs to a site (Hopmans et al., 2004; Weijers et al., 2006) and Methane Index (Zhang et al., 2011). Regarding the backtracking simulation, we also we recommend areas of further research: (1) running a trajectory simulation of the GDGTs before sinking to compare with our result. (2) considering a depth productivity of GDGTs the water column which can be used as a standard to determine the sub-SST bias. This can be useful for further research to prove if TEX_{86} reflects the subsurface temperature, not SST (3) Local events (for instance, El Niño–Southern Oscillation) on South Atlantic could also be included, which might influence the result in a relation to climate variability (Nooteboom et al., 2019) (4) Simulation for a global scale to have a completed coverage and see if there is an anomaly that deviates from what is standard, normal or expected at a certain time or place.

In general, it is logical to consider the water depth as a specific parameter to identify sensitivity to lateral transport since there is more chance for lateral transports with an increasing sinking time. However, it not necessarily true because the lateral transport can cause an elevated bias even in shallow sites. However, the simulation proved that prevailing ocean currents could be a characteristic

which becomes important, especially the current crossing a large temperature gradient, resulting in the larger offset.

4. CONCLUSION

The effect of the horizontal transport on GDGTs-bearing particles in ocean currents on sedimentary signals in microfossil assemblages for reconstructing past climate has been studied via particle modeling, called OceanParcels. The sources of scatter contributing to a deviation in the TEX_{86} calibration were identified, and it was found that the increasing ([2]/[3]) with depth, suggesting that there is contribution from Archaea living in the deeper water column due to export dynamics influencing GDGT-derived SST estimates. This influence can be seen because those two datasets (Global, Regional) have varying depth transect and temperature range. However, it is notable that lateral transport influence is perceptible after dividing the basin into specific clusters, and locations, where the particles were transported, were observed specifically in the Southeast and the Southwest Atlantic. The Southeast Atlantic is subjected to Agulhas Current while the Southwest Atlantic is induced by two currents (the Malvinas Current from the Southern Ocean and the Brazil Current from the Equatorial Current) leading to cold bias in this region. Hence, it is sensible to conclude that lateral transport by currents also governs the sedimentary assemblage distribution as a paleoceanographic proxy. Again, [2]/[3] ratio shows a strong correlation with ΔSST Bias; this is consistent with the depth being higher with an increasing water column, meaning that the depth of the production of Thaumarchaeota generally contributes more than the lateral transport.

5. ACKNOWLEDGEMENTS

I would like to thank to my supervisors Dr. Ir. Francien Peterse and Dr. Peter Bijl of Earth Science Department of Geoscience Faculty for their instruction and support throughout this thesis project. I thank Addison Rice for the technical assistance. I also thank Peter Nooteboom, M.Sc and Dr. Erik van Sebille (IMAU) for using the Parcel Model to do simulation. I am grateful for the insightful and thorough comments which resulted in many improvements to the manuscript. I thank to Jessica E Tierney and Martin P Tingley for providing the TEX_{86} data calibration. I would also like to express thank to Indonesia Endowment Fund for Education (LPDP) for the funding during my study. Finally, I am extremely grateful for this research opportunity during this pandemic.

References

Anderson, D. M., Lively, J. J., Reardon, E. M., & Price, C. a. (1985). Sinking characteristics of dinoflagellate cysts. Limnology and Oceanography, 30(5), 1000–1009. https://doi.org/10.4319/lo.1985.30.5.1000

Charlotte L. O'Brien, Stuart A. Robinson, Richard D. Pancost, Jaap S. Sinninghe Damsté, Stefan Schouten, Daniel J. Lunt, Heiko Alsenz, André Bornemann, Cinzia Bottini, Simon C. Brassell, Alexander Farnsworth, Astrid Forster, Brian T. Huber, Gordon N. Inglis, Hugh C. Jenkyns, Christian Linnert, Kate Littler, Paul Markwick, Alison McAnena, Jörg Mutterlose, B. David A. Naafs, Wilhelm Püttmann, Appy Sluijs, Niels A.G.M. van Helmond, Johan Vellekoop, Thomas Wagner, Neil E. Wrobel (2018) Cretaceous sea-surface temperature evolution: Constraints from TEX_{86} and planktonic foraminiferal oxygen isotopes. Earth-Science Reviews. 172, 224-247. https://doi.org/10.1016/j.earscirev.2017.07.012

Carme Huguet, Jung-Hyun Kim, Jaap S. Sinninghe Damsté, Stefan Schouten. (2006). Reconstruction of sea surface temperature variations in the Arabian Sea over the last 23 kyr using organic proxies (TEX_{86} and $U_{37}^{K'}$). Paleoceanography and Paleoclimatology. https://doi.org/10.1029/2005PA001215

De la Torre, J. R., Walker, C. B., Ingalls, A. E., Könneke, M., & Stahl, D. A. (2008). Cultivation of a thermophilic ammonia oxidizing archaeon synthesizing crenarchaeol. Environmental microbiology, 10(3), 810-818.

De Rosa, M., Esposito, E., Gambacorta, A., Nicolaus, B., & Bu'Lock, J. D. (1980). Effects of temperature on ether lipid composition of Caldariella acidophila. Phytochemistry, 19(5), 827-831.

DeLong, E. F., King, L. L., Massana, R., Cittone, H., Murray, A., Schleper, C., & Wakeham, S. G. (1998). Dibiphytanyl ether lipids in nonthermophilic crenarchaeotes. Applied and Environmental Microbiology, 64(3), 1133-1138.

Elling, F.J., Könneke, M., Lipp, J.S., Becker, K.W., Gagen, E.J., Hinrichs, K.-U., 2014. Effects of growth phase on the membrane lipid composition of the thaumarchaeon Nitrosopumilus maritimus and their implications for archaeal lipid distributions in the marine environment. Geochim. Cosmochim. Acta 141, 579–597.

Elling, F.J., Könneke, M., Mußmann, M., Greve, A., Hinrichs, K.-U., 2015. Influence of temperature, pH, and salinity on membrane lipid composition and TEX_{86} of marine planktonic thaumarchaeal isolates. Geochim. Cosmochim. Acta 171, 238–255.

Inglis, G.N., Farnsworth, A., Lunt, D., Foster, G.L., Hollis, C.J., Pagani, M., Jardine, P.E., Pearson, P.N., Markwick, P., Galsworthy, A.M.J., Raynham, L., Taylor, K.W.R., Pancost, R.D., 2015. Descent towards the icehouse: Eocene sea surface cooling in- ferred from GDGT distributions. Paleoceanography 29, 1000–1020. http://dx.doi.org/10.1002/2014PA002723.

Ho, S.L., Yamamoto, M., Mollenhauer, G., Minagawa, M., 2011. Core top TEX86 values in the south and Equatorial Pacific. Organic Geochemistry 42, 94–99.

Ho, S.L., Mollenhauer, G., Fietz, S., Martínez-Garcia, A., Lamy, F., Rueda, G., Schipper, K., Méheust, M., Rosell-Melé, A.,Stein, R., 2014. Appraisal of TEX_{86} and thermometries in subpolar and polar regions. Geochim. Cosmochim. Acta 131, 213–226.

Ho, S.L., Laepple, T., 2016. Flat meridional temperature gradient in the early Eocene in the subsurface rather than surface ocean. Nat. Geosci. 9, 606–610.

Hopmans, E. C. et al. A novel proxy for terrestrial organic matter in sediments based on branched and isoprenoid tetraether lipids. Earth Planet. Sci. Lett. 224, 107–116 (2004).

Hu, A.Y., Jiao, N.Z., Zhang, C.L., 2011a. Community structure and function of planktonic Crenarchaeota: changes with depth in the South China Sea. Microbial Ecology 62, 549–563.

Hu, A.Y., Jiao, N.Z., Zhang, R., Yang, Z., 2011b. Niche partitioning of marine group I Crenarchaeota in the euphotic and upper mesopelagic zones of the East China Sea. Applied and Environmental Microbiology 77, 7469–7478.

Hurley, S.J., Elling, F.J., Könneke, M., Buchwald, C., Wankel, S.D., Santoro, A.E., Lipp, J.S., Hinrichs, K.-U., Pearson, A., 2016. Influence of ammonia oxidation rate on thaumarchaeal lipid composition and the TEX_{86} temperature proxy. Proc. Natl. Acad. Sci. 113, 7762–7767.

Pierini, Jorge, Michelle Lovallo, Eduardo Gómez, Luciano Telesca, Luciano (2016) Fisher–Shannon analysis of the time variability of remotely sensed sea surface temperature at the Brazil–Malvinas Confluence – 58. 10.1016/j.oceano.2016.02.003. Oceanologia

Kim J.-H., Schouten S., Hopmans E. C., Donner B. and Sinninghe Damste ´ J. S. (2008) Global sediment core-top calibration of the TEX_{86} paleothermometer in the ocean. Geochim. Cosmochim. Acta72, 1154–1173.

Kim J., Xavier Crosta, Elisabeth Michel, Stefan Schouten, Josette Duprat, Jaap S. Sinninghe Damsté. 2009. Impact of lateral transport on organic proxies in the Southern Ocean, Quaternary.71, 246-250. Htps://doi.org/10.1016/j.yqres.2008.10.005.

Kim J., Van der Meer J., Schouten S., Helmke P., Willmott V., Sangiorgi F., Koc N., Hopmans E. andSinninghe Damste ´ J. (2010) New indices and calibrations derived from the distribu- tion of crenarchaeal isoprenoid tetraether lipids: Implications for past sea surface temperature reconstructions.Geochim. Cosmochim. Acta 74, 4639–4654.

Kim, J.-H., Crosta, X., Willmott, V., Renssen, H., Bonnin, J., Helmke, P., Schouten, S., Sinninghe Damsté, J.S., 2012a. Holocene subsurface temperature variability in the eastern Antarctic continental margin. Geophysics Research Letters 39, L06705.

Kim, J.-H., Romero, O.E., Lohmann, G., Donner, B., Laepple, T., Haam, E., SinningheDamsté, J.S., 2012b. Pronounced subsurface cooling of North Atlantic waters off Northwest Africa during Dansgaard–Oeschger interstadials. Earth and Planetary Science Letters 229–240, 95–102.

Kim, J.-H., Stefan Schouten, Marta Rodrigo-Gámiz, Sebastiaan Rampen, Gianluca Marino, Carme Huguet, Peer Helmke, Roselyne Buscail, Ellen C. Hopmans, Jörg Pross, Francesca Sangiorgi, Jack B.M. Middelburg, Jaap S. Sinninghe Damsté. influence of deep-water derived isoprenoid tetraether lipids on the paleothermometer in the Mediterranean Sea. Geochimica et Cosmochimica Acta 150, 125–141 (2015).

Ksepka, Daniel and Thomas, Daniel (2011). Multiple Cenozoic invasions of Africa by penguins (Aves, Sphenisciformes). Proceedings. Biological sciences / The Royal Society.279, 1027-32 Http://doi.org10.1098/rspb.2011.1592

Lee, K.E., Kim, J.-H., Wilke, I., Helmke, P., Schouten, S., 2008. A study of the alkenone, TEX86, and planktonic foraminifera in the Benguela upwelling system: implications for past sea surface temperature estimates. Geochemistry, Geophysics, Geosystems 9, 1–19.

Lopes dos Santos, R., Prange, M., Castañeda, I.S., Schefuß, E., Mulitza, S., Schulz, M., Niedermeyer, E.M., Sinninghe Damsté, J.S., Schouten, S., 2010. Glacial-interglacial var- iability in Atlantic meridional overturning circulation and thermocline adjustments in the tropical North Atlantic. Earth and Planetary Science Letters 300, 407–414.

Massana R., DeLong E. F. and Pedros-Alio C. (2000) A few cosmopolitan phylotypes dominate planktonic archaeal assemblages in widely different oceanic provinces. Appl. Environ. Microbiol. 66, 1777–1787.

Matano, R. P., Palma, E. D., & Piola, A. R. (2010). The influence of the Brazil and Malvinas Currents on the Southwestern Atlantic Shelf circulation. Ocean Science, 6(4), 983–995. https://doi.org/10.5194/os-6-983-2010.

Mincer T. J., Church M. J., Taylor L. T., Preston C., Karl D. M. and DeLong E. F. (2007) Quantitative distribution of presumptive archaeal and bacterial nitrifiers in Monterey Bay and the North Pacific Subtropical Gyre. Environ. Microbiol. 9, 1162–1175.

Mollenhauer G., Eglinton T. I., Hopmanns E. C. and Sinninghe Damste ´ J. S. (2008) A radiocarbon-based assessment of the preservation characteristics of crenarchaeol and alkenones from continental margin sediments. Org. Geochem. 99, 1039–1045. Ocean Color Web: <http://oceancolor.gfs.nasa.gov> (July 2012)

M.T. Hernández-Sánchez, E.M.S. Woodward, K.W.R. Taylor, G.M. Henderson, R.D. Pancost, Variations in GDGT distributions through the water column in the South East Atlantic Ocean, Geochimica et Cosmochimica Acta, Volume 132, 2014, Pages 337-348, ISSN 0016-7037, https://doi.org/10.1016/j.gca.2014.02.009.

Nooteboom, P. D., Bijl, P. K., Sebille, E., Heydt, A. S., & Dijkstra, H. A. (2019). Transport bias by ocean currents in sedimentary microplankton assemblages: Implications for paleoceanographic reconstructions. Paleoceanography and Paleoclimatology, 34, 1178-1194, https://doi.org/10.1029/2019PA003606

Pitcher, A., Rychlik, N., Hopmans, E. C., Spieck, E., Rijpstra, W. I. C., Ossebaar, J. & Damsté, J. S. S.(2010). Crenarchaeol dominates the membrane lipids of Candidatus Nitrososphaera gargensis, a thermophilic Group I. 1b Archaeon. The ISME Journal, 4(4), 542-552.

Qin, W., Carlson, L.T., Armbrust, E.V., Devol, A.H., Moffett, J.W., Stahl, D.A., Ingalls, A.E., 2015. Confounding effects of oxygen and temperature on the TEX_{86} signature of marine Thaumarchaeota. Proc. Natl. Acad. Sci. 112, 10979–10984.

Schouten, S., Hopmans, E. C., Schefuß, E., & Damste, J. S. S. (2002). Distributional variations in marine crenarchaeotal membrane lipids: a new tool for reconstructing ancient sea water temperatures? Earth and Planetary Science Letters, 204(1-2), 265-274.

Schouten, S., Astrid Forster, F. Elda Panoto, Jaap S. Sinninghe Damsté (2007) Towards calibration of the TEX_{86} palaeothermometer for tropical sea surface temperatures in ancient greenhouse worlds. Org. Geochem. Volume 38, Issue 9, Pages 1537-1546,

Schouten, S., Hopmans, E. C., Van Der Meer, J., Mets, A., Bard, E., Bianchi, T. S., ... & Huguet, C. (2009). An interlaboratory study of TEX_{86} and BIT analysis using high-performance liquid chromatography–mass spectrometry. Geochemistry, Geophysics, Geosystems, 10(3).

Schouten, S., Hopmans, E. C., & Damsté, J. S. S. (2013). The organic geochemistry of glycerol dialkyl glycerol tetraether lipids: a review. Organic geochemistry, 54, 19-61

Sinninghe Damsté, J.S., Schouten, S., Verschuren, D., 2012. Distribution of tetraether lipids in the 25-ka sedimentary record of Lake Challa: extracting reliable TEX_{86} and MBT/CBT palaeotemperatures from an equatorial African lake. Quat. Sci. Rev. 50, 43–54.

Majumder, Sudip., and Claudia Schmid. 2017. A Study of the Variability of the Benguela Current. Ocean Science Discussions. 10.5194/os-2017-63

Taylor, K. W. R., Huber, M., Hollis, C. J., Hernandez Sanchez, M. T., & Pancost, R. D. (2013). Re- evaluating modern and Palaeogene GDGT distributions: Implications for SST reconstructions. Global and Planetary Change, 108, 158-174. https://doi.org/10.1016/j.gloplacha.2013.06.011

Tierney, J. E., & Tingley, M. P. (2014). A Bayesian, spatially-varying calibration model for the TEX_{86} proxy. Geochimica et Cosmochimica Acta, 127, 83106. https://doi.org/10.1016/j.gca.2013.11.026

Tierney, J.E., Tingley, M.P., 2015. A TEX_{86} surface sediment database and extended Bayesian calibration. Sci. Data 2, 150029. http://dx.doi.org/10.1038/sdata.2015.29.

Tierney, J. E., Sinninghe Damsté, J. S., Pancost, R. D., Sluijs, A. & Zachos, J. C. Eocene temperature gradients. Nat. Geosci. 10, 538 (2017).

Trommer, G., Siccha, M., van der Meer, M.T., Schouten, S., Sinninghe Damsté, J.S., Schulz, H., Hemleben, C., Kucera, M., 2009. Distribution of Crenarchaeota tetraether membrane lipids in surface sediments from the Red Sea. Org. Geochem. 40, 724–731.

Uda, I., Sugai, A., Itoh, Y. H., & Itoh, T. (2001). Variation in molecular species of polar lipids from Thermoplasma acidophilum depends on growth temperature. Lipids, 36(1), 103-105.

Uda, I., Sugai, A., Itoh, Y. H., & ITOH, T. (2004). Variation in molecular species of core lipids from the order Thermoplasmales strains depends on the growth temperature. Journal of Oleo Science, 53(8), 399- 404.

Van Sebille, E., Griffies, S. M., Abernathey, R., Adams, T. P., Berloff, P., Biastoch, A., et al. (2018). Lagrangian ocean analysis: Fundamentals and practices. Ocean Modelling, 121, 49–75. https://doi.org/10.1016/j.ocemod.2017.11.008

Wakeham, S.G., Lewis, C.M., Hopmans, E.C., Schouten, S., Sinninghe Damsté, J.S., 2003. Archaea mediate anaerobic oxidation of methane in deep euxinic waters of the Black Sea. Geochim. Cosmochim. Acta 67, 1359–1374.

Weijers, J. W. H., Schouten, S., Spaargaren, O. C., & Sinnige Damsté, J. S. (2006). Occurrenceand distribution of tetraether membrane lipids in soils: implications for the use of the TEX_{86} proxy and the BIT index. Organic Geochemistry, 37(12), 1680-1693. https://doi.org/10.1016/j.orggeochem.2006.07.018

Wuchter, C., Schouten, S., Coolen, M. J., & Sinninghe Damsté, J. S. (2004). Temperature-dependent variation in the distribution of tetraether membrane lipids of marine Crenarchaeota: Implications for TEX_{86} paleothermometry. Paleoceanography, 19(4)

Wuchter, C., Schouten, S., Wakeham, S.G., Sinninghe Damsté, J.S., 2005. Temporal and spatial variation in tetraether membrane lipids of marine Crenarchaeota in particu- late organic matter: implications for TEX_{86} paleothermometry. Paleoceanography 20, PA3013. http://dx.doi.org/10.1029/2004PA001110.

Wuchter C., Schouten S., Wakeham S. G. and Sinninghe ´ Damste ´ J. S. (2006) Archaeal tetraether membrane lipid fluxes in the northeastern Pacific and the Arabian Sea: implications for TEX_{86} paleothermometry. Paleoceanography 21, PA4208. http://dx.doi.org/10.1029/2006PA001279.

Zhang, Y.G., Zhang, C.L., Liu, X.-L., Li, L., Hinrichs, K.-U., Noakes, J.E., 2011. Methane index: a tetraether archaeal lipid biomarker indicator for detecting the instability of marine gas hydrates. Earth Planet. Sci. Lett. 307, 525–534.

Zhang, Y. G., M. Pagani, and Z. Wang (2016), Ring Index: A new strategy to evaluate the integrity of TEX_{86} paleothermometry, Paleoceanography, 31, 220–232, doi:10.1002/ 2015PA002848.

Zonneveld, K., Marret, F., Versteegh, G., Bogus, K., Bonnet, S., Bouimetarhan, I., et al. (2013a). Geographic distribution of dinoflagellate cysts in surface sediments. PANGAEA, https://doi.org/10.1594/PANGAEA.818280

Appendix

A. Trajectory Simulation

A.1 The OceanParcels

Parcels (Probably A Really Computationally Efficient Lagrangian Simulator) is a set of Python classes and methods used to create customizable particle tracking simulations using output of the Ocean Circulation models. Parcels can be used for tracking passive and active particulates such as water, plankton, plastic and fish. The code of the OceanParcels project is licensed under an open source MIT license (downloaded from github.com/OceanParcels/parcels or installed via anaconda. org/conda-forge/parcels:

The easiest way to install Parcels code is by using Anaconda and Parcels Conda-Forge package with the current release of Parcels. This package will automatically install all the requirements for a fully functional installation of Parcels. This is the “batteries-included” solution probably suitable for most users.

Source: http://oceanparcels.org/

A.2 NEMO

NEMO stands for "Nucleus for European Modelling of the Ocean" is the latest modelling framework developed by European consortium in a sustainable manner for marine and climate scientific research activities and forecasting services

The NEMO ocean model consists of three main components:

- NEMO-OCE models the ocean {thermo}dynamics and solves the primitive equations
- NEMO-ICE (SI^3: Sea-Ice Integrated Initiative) models sea-ice {thermo}dynamics, brine inclusions and subgrid-scale thickness variations
- NEMO-TOP (Tracers in the Ocean Paradigm) models the {on,off}line oceanic tracers transport and biogeochemical processes (using PISCES)

Source: https://www.nemo-ocean.eu/

B. Figures

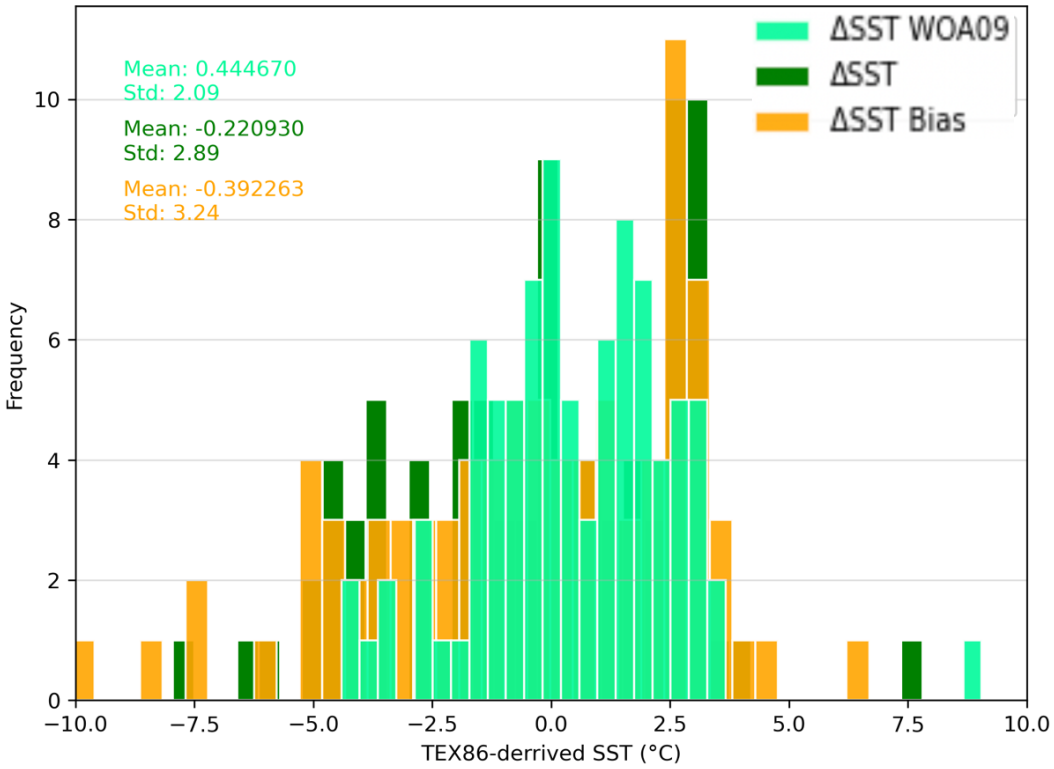

A

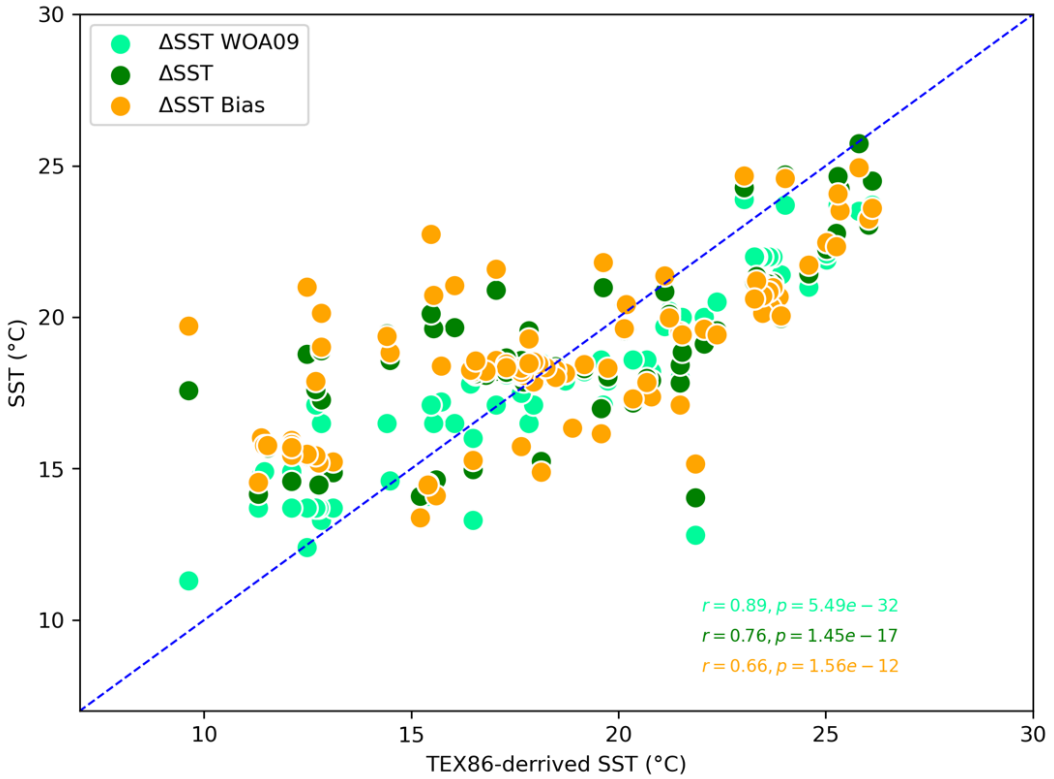

B

Figure B. 1 Fig. 3 The TEX86 Calibration plots. Normal Distribution based on the calibration. A) The light and dark green bar represents ΔSST from WOA09 and TEX86-derived SST – directly-overlying SST, respectively. The orange bar represents ΔSST Bias, derived from TEX86-derived – lateral transport-related SST). B) a strong relation by using Pearson Correlation Coefficient.

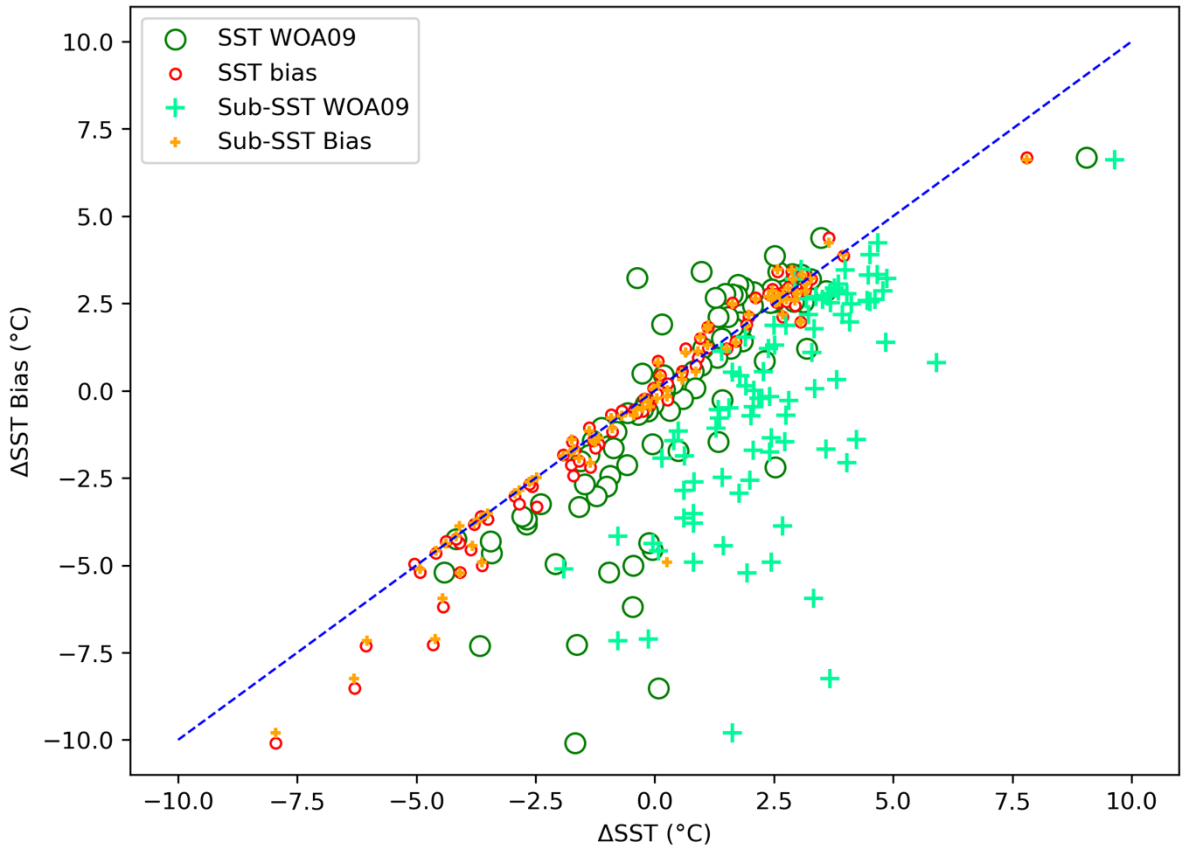

Figure B. 2 The Relationship between ΔSST and its bias due to Lateral Transport with modeled SST and WOA09 presenting in SST and sub-SST data

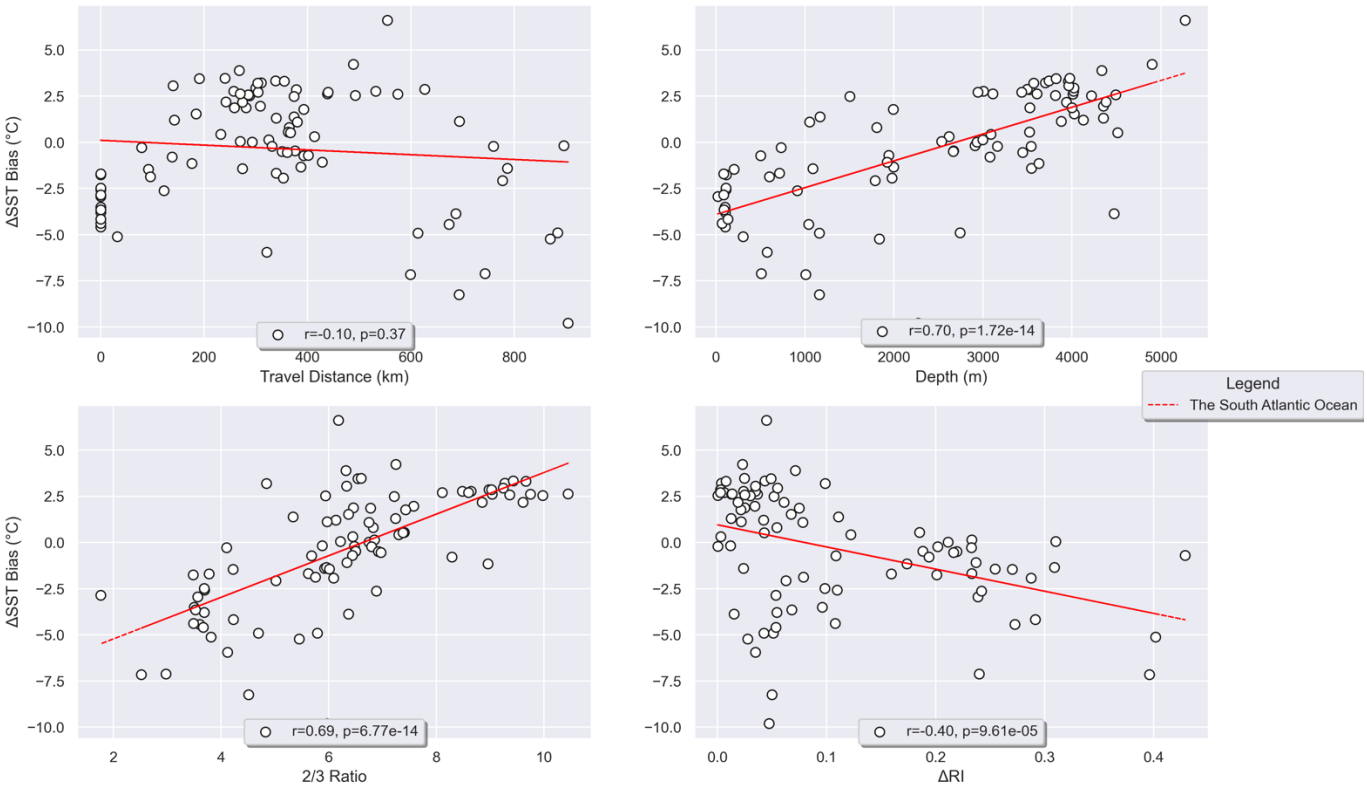

Figure B. 3 The correlation of ΔSST Bias in the sub-SSTs due to lateral transport over four possible sources in the South Atlantic Ocean (A. Travel Distance, B. Depth, C. [2]/[3] Ratio, D. ΔRI).

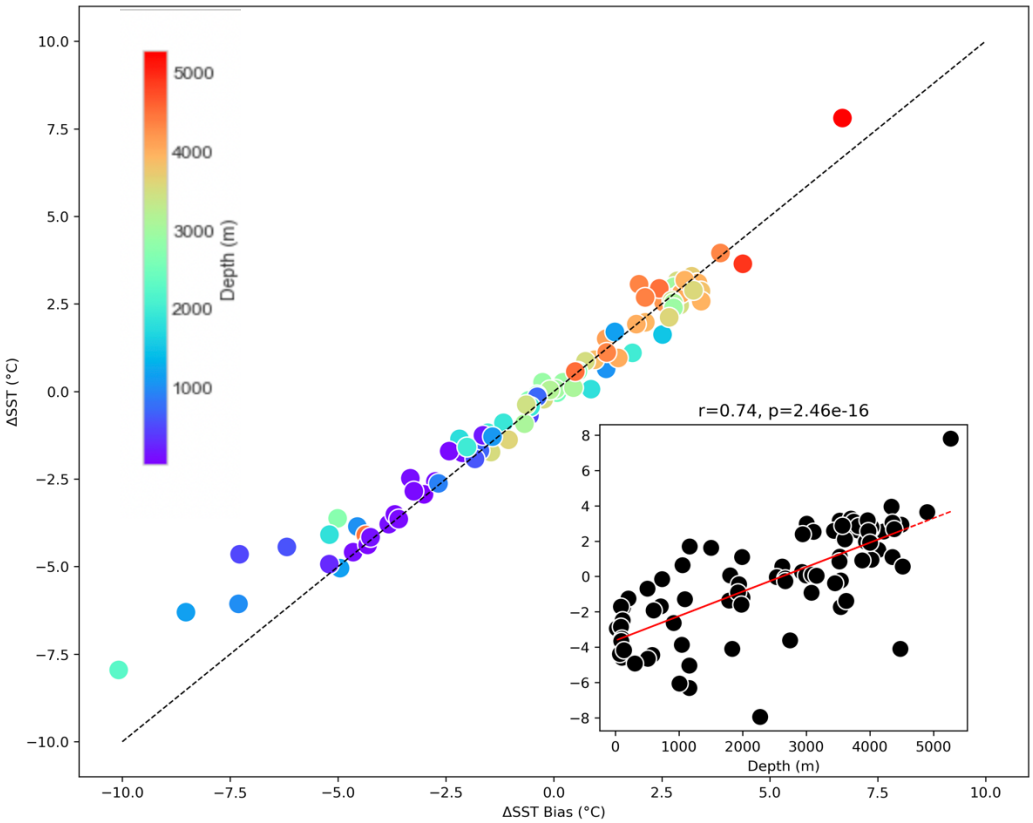

Figure B. 4 The correlation of ΔSST and depth in the South Atlantic Ocean

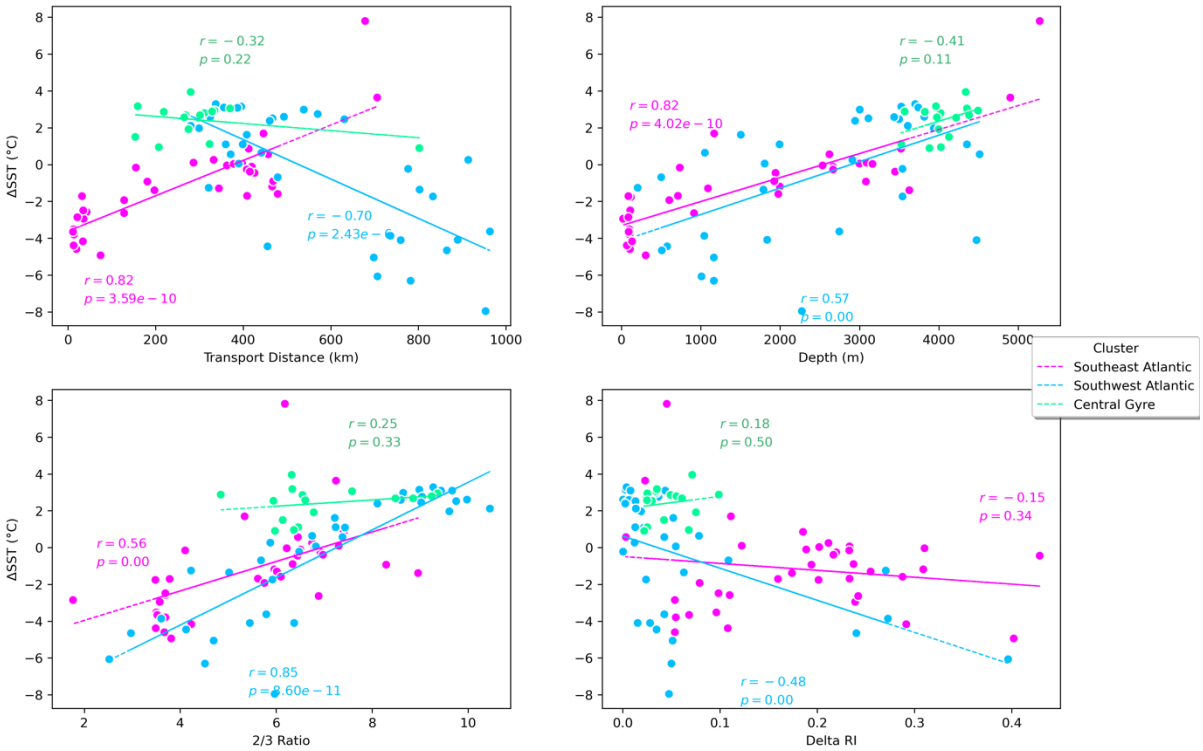

Figure B. 5 The correlation of ΔSST over four possible Sources A) Travel Distance; B) Depth; C) [2]/[3] Ratio; D) ΔRI, in three main region: Southeast Atlantic (Pink dot), Southwest Atlantic (Blue dot), and Central Gyre (Green dot).

C. Pearson Correlation

The correlation coefficient is used to measure how strong the relationship between two variables. There are several types of correlation coefficients, but the most popular is Pearson's. Pearson's correlation coefficient, also known as Pearson's R, is a correlation coefficient commonly used in linear regression. Starting to work in statistics, people may first understand Pearson's R. In fact, when anyone mentions correlation coefficient, they are usually talking about Pearson's correlation coefficient.

The value returned by the formula is between -1 and 1, where:

- a strong positive relationship is indicated by 1
- a strong negative relationship is highlighted by -1
- a result of zero means it does not matter at all.

Pearson's correlation coefficient formula is shown as follows.

$$r = \frac{n(\Sigma xy) - (\Sigma x)(\Sigma y)}{\sqrt{[\, n\Sigma x^2 - (\Sigma x)^2 \,][\, n\Sigma y^2 - (\Sigma y)^2 \,]}}$$

Source: https://www.statisticshowto.com/probability-and-stati yesstics/correlation-coefficient-formula/#Pearson